

Copyright

by

Stephen Christopher Johnson

1999

Selectively Compliant Orientation Stages for Imprint Lithography

by

Stephen Christopher Johnson, B.S.

Thesis

Presented to the Faculty of the Graduate School

of The University of Texas at Austin

in Partial Fulfillment

of the Requirements

for the Degree of

Master of Science in Engineering

The University of Texas at Austin

May 1999

Selectively Compliant Orientation Stages for Imprint Lithography

Approved by
Supervising Committee:

Acknowledgments

This work would not have been possible without the advice and support of many people. I would like to thank my advisor, Professor S.V. Sreenivasan for his guidance and support throughout my graduate career. I would also like to thank Professor Grant Willson for sharing his extensive knowledge of the semiconductor industry and teaching by example. I learned a great deal about spatial kinematics from Jin Choi, and I greatly enjoyed our numerous conversations over a cup of coffee. Thanks to Matt Colburn for all of his efforts in developing the first SFIL imprint machine. Thanks to Don Artieschoufsky, Danny Jarez, and everyone in the mechanical engineering machine shop for sharing their wisdom and advice. I would also like to thank Ulratech Stepper, Etec, IBM-Burlington, and Professor Jack Wolfe's group at the University of Houston for technical contributions to this work. Thanks to the SRC and DARPA for financial support. Finally, thanks to all of my colleagues on the Step and Flash project. I have enjoyed working with you, and my graduate school experience would not have been the same without you.

May 3, 1999

Selectively Compliant Orientation Stages for Imprint Lithography

by

Stephen Christopher Johnson, M.S.E.

The University of Texas at Austin, 1999

Supervisor: S. V. Sreenivasan

This document investigates the motion capability of partially constrained compliant spatial mechanisms. The investigation is directed towards the design of partially constrained orientation stages for a new imprint lithography process known as Step and Flash Imprint Lithography. This text begins with an introduction to this new imprint lithography technology and continues with an investigation of the compliance matrix eigenvalue problem to compare two imprint lithography orientation stages. The eigenvalues and eigenvectors of a compliant structure's compliance matrix can provide insight into a structure's behavior when loaded. The eigenstructure is shown to be effective for examining the motions of unconstrained or ideal compliant structures. Characterization of structures that are both partially constrained and non-ideal requires the use of an alternative metric, that of strain energy imparted to the system. The eigenvalue problem of these stages is ill-conditioned due to the presence of eigenvalues that are nearly zero and an eigenvector space that is near-defective. Two orientation stage designs are shown to have appropriate motion capabilities for imprint lithography applications. The development of a prototype imprint lithography machine is described, and experimental results of imprint lithography demonstrations are included.

Table of Contents

LIST OF FIGURES.....	viii
1 INTRODUCTION.....	1
1.1 OPTICAL LITHOGRAPHY.....	1
1.1.1 Process Description.....	2
1.1.2 Technical Challenges.....	3
1.2 IMPRINT LITHOGRAPHY.....	4
1.2.1 Imprint Lithography Process Description.....	5
1.2.2 Technical Challenges.....	6
1.3 STEP AND FLASH IMPRINT LITHOGRAPHY.....	7
1.3.1 Template Generation.....	7
1.3.2 Step and Flash Lithography Process Description.....	8
1.3.3 Technical Challenges.....	10
2 IMPRINT MACHINE DESIGN.....	12
3 ORIENTATION STAGE DEVELOPMENT.....	15
3.1 INTRODUCTION TO SCREW SYSTEM THEORY.....	16
3.1.1 Screw axis ($\$$).....	17
3.1.2 Motor ($\hat{\mathbf{v}}$).....	19
3.1.3 Wrench ($\hat{\mathbf{f}}$).....	19
3.1.4 Reciprocity.....	19
3.2 FIRST GENERATION ORIENTATION STAGE.....	21
3.2.1 Mobility Analysis.....	21
3.2.2 Detailed Design.....	23
3.3 THE USE OF FLEXURES IN MECHANISM DESIGN.....	25
3.4 SECOND GENERATION LUMPED FLEXURE STAGE.....	27
3.4.1 Mobility Analysis.....	27
3.4.2 Detailed Design.....	29
3.5 THIRD GENERATION DISTRIBUTED FLEXURE STAGE.....	29
4 MOBILITY ANALYSIS.....	33

4.1	BASIS OF COMPARISON	33
4.1.1	<i>Wrenches, Twists, and the Compliance Matrix</i>	33
4.2	IDEAL KINEMATIC STAGE	36
4.2.1	<i>Compliance Matrix</i>	36
4.2.2	<i>Eigenscrews and Eigenvalues</i>	40
4.3	DISTRIBUTED FLEXURE STAGE.....	42
4.3.1	<i>Finite Element Model</i>	42
4.3.2	<i>Analysis of Wrench and Twist Matrices</i>	46
4.3.3	<i>Eigenvalues and Eigenvectors</i>	48
4.3.4	<i>The Use of Strain Energy as a Metric</i>	54
4.4	SUMMARY.....	56
5	EXPERIMENTAL RESULTS	57
5.1	IMAGES ON FLAT SUBSTRATES.....	57
5.2	IMAGES ON CURVED SUBSTRATES	59
6	CLOSING REMARKS.....	61
6.1	CONCLUSIONS	61
6.2	FUTURE WORK.....	62
6.2.1	<i>Base Layer Thickness</i>	62
6.2.2	<i>Scientific Investigation</i>	64
6.2.3	<i>Sensing</i>	64
6.2.4	<i>Active and Passive Stages</i>	65
6.2.5	<i>Overlay</i>	66
6.2.6	<i>Template Loading and Deformation</i>	66
	APPENDIX A	67
	APPENDIX B	69
	REFERENCES.....	78
	VITA.....	80

List of Figures

FIGURE 1.1 OPTICAL LITHOGRAPHY PROCESS	2
FIGURE 1.2 IMPRINT LITHOGRAPHY PROCESS	5
FIGURE 1.3 IMPRINT LITHOGRAPHY PATTERN DENSITY DEPENDENCE	7
FIGURE 1.4 STEP AND FLASH IMPRINT LITHOGRAPHY PROCESS	9
FIGURE 2.1 STEP AND FLASH PRESS	13
FIGURE 3.1 ANGULAR MISALIGNMENT BETWEEN TEMPLATE AND MASK	15
FIGURE 3.2 DESIRED AND UNDESIRED MOTIONS BETWEEN TEMPLATE AND WAFER	16
FIGURE 3.3 THE GEOMETRY OF THE VELOCITY FIELD OF POINTS IN A RIGID BODY	18
FIGURE 3.4 A RECIPROCAL WRENCH, $\hat{\mathbf{f}}$, APPLIED TO A BODY WITH 5TH ORDER MOTION SCREW	20
FIGURE 3.5 IDEAL ORIENTATION STAGE KINEMATIC MODEL	21
FIGURE 3.6 WRENCHES RECIPROCAL TO ORIENTATION STAGE	22
FIGURE 3.7 INITIAL WAFER ORIENTATION STAGE	24
FIGURE 3.8 REVOLUTE JOINT AND CORRESPONDING FLEXURE	25
FIGURE 3.9 LUMPED FLEXURE STAGE	27
FIGURE 3.10 WRENCHES RECIPROCAL TO LUMPED FLEXURE STAGE	28
FIGURE 3.11 DISTRIBUTED FLEXURE ORIENTATION STAGE	30
FIGURE 3.12 FIXED-FIXED BEAM	31
FIGURE 4.1 SCREW REPRESENTATION OF THREE LEG MODEL	37
FIGURE 4.2 FINITE ELEMENT MODEL	44
FIGURE 4.3 DEFLECTED FINITE ELEMENT MODEL	45
FIGURE 4.4 FLEXURE STAGE COORDINATE FRAME	47
FIGURE 5.1 AFM IMAGE OF 20 μm FEATURE	57
FIGURE 5.2 AFM IMAGE OF SUB-MICRON LINES AND SPACES	58
FIGURE 5.3 60 NM FEATURES ON TEMPLATE* AND ETCH BARRIER	58
FIGURE 5.4 150 NM FEATURES IN ETCH BARRIER	59
FIGURE 5.5 OPTICAL MICROGRAPHS OF IMAGES ON CURVED TEMPLATE AND SUBSTRATE	60
FIGURE 5.6 SEM AND AFM IMAGES OF PATTERNED SPHERICAL SUBSTRATE	60
FIGURE 6.1 RESIDUAL BASE LAYER	62

1 Introduction

The parallel transfer of high-resolution patterns over large areas has become a focal point of research in the semiconductor industry. The process of transferring sub-micron features onto wafers, referred to as lithography, is one of the key technologies in manufacturing semiconductor devices. Circuits with small components operate at high speeds. Smaller circuits also allow semiconductor manufacturers to increase profits by placing more circuits on one wafer. These economic forces have driven the microelectronics industry to invest hundred of millions of dollars in researching next generation lithography techniques.

Optical lithography currently satisfies manufacturers' requirements and is the process of choice for semiconductor companies. 0.2 micron devices are currently manufactured with optical lithography. However, may believe that optical limits hinder the cost-effective generation of circuits with still smaller components. The Semiconductor Industry Association Roadmap outlines cost and timetables for developing alternative lithography techniques capable of imaging features smaller than 100 nm. This chapter describes the optical lithography process, examines some of the limitations of optical lithography, and presents two alternative high-resolution pattern transfer technologies.

1.1 Optical Lithography

The semiconductor industry currently uses optical lithography to produce integrated circuits. This well established process generates patterns on silicon wafers using an optical projection technique. A layer of photosensitive polymer absorbs an aerial image that is then chemically transferred to the wafer.

1.1.1 Process Description

Figure 1.1 illustrates the optical lithography process. To begin the process, a silicon wafer is spin coated with photoresist. Photoresist is an organic polymer that captures an optical image projected onto it. The imaged photoresist is then used to mask the silicon wafer during subsequent manufacturing steps.

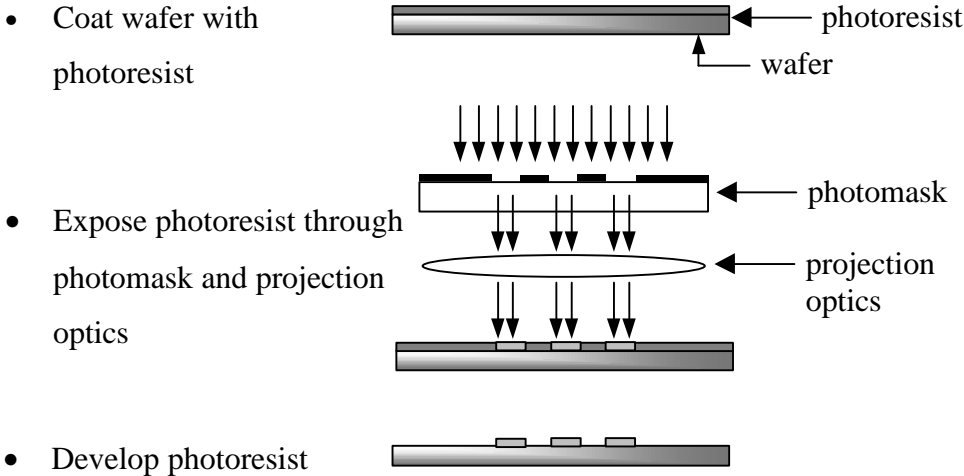


Figure 1.1 Optical lithography process

A patterned layer of chromium on a quartz photomask defines the master circuit image to be transferred to the wafer. The photomask is placed above a wafer and its top surface is illuminated. When a light source illuminates the top of the photomask, the pattern written in the chromium is projected onto the wafer below.

The imaging layer captures the aerial image projected onto the wafer. Light alters the chemical structure of the photoresist and changes its solubility. Rinsing the wafer in a developer solution selectively dissolves the photoresist. This rinse leaves a layer of photoresist in the shape of the circuit pattern that was written on the photomask.

Once the photomask has been patterned, it serves as an etch or ion implantation mask. A chemical etch removes areas of underlying substrate not protected by the patterned photoresist. The remaining photoresist is then stripped from the wafer. The end result of this process is a pattern transfer into the substrate. These patterns in resist are used to control the patterning and placement of various steps required to manufacture a microelectronic circuit.

1.1.2 Technical Challenges

Diffraction limits the production of small features with optical lithography. Much of the technological investment in lithography tools goes into optical projection systems designed to minimize the effect of diffraction. The numerical aperture of the lens, the wavelength of light, and the chemical development process determine the minimum line width that a lithography tool can print (Thompson, 1994):

$$LW = \frac{k\lambda}{NA} \quad (1.1)$$

where

LW is the minimum printable line width (nm)

NA is the numerical aperture of the lens in the stepper

k is a factor describing the photoresist and development process

λ is the wavelength of light used in the printing process (nm)

Thus, the minimum printable line width may be decreased by increasing the numerical aperture of the lens, improving processing of the resist, or decreasing the wavelength of light used to print. Typical k values for resist technology range from 0.8 for standard procedures to 0.6 for complex multi-layer resist processes [Thompson, 1994].

The numerical aperture of a lens is a measure of what angle light may enter the lens. Increasing the numerical aperture of a lens while maintaining allowable field sizes, requires must increasing the size of the lens. Large lenses are more difficult to manufacture and, thus, more expensive. It is not uncommon for lens systems in today's step and repeat photolithography tools to weigh hundreds of pounds and cost several million dollars.

Investments in reducing the wavelength of light used to print images have reduced minimum printable line widths. Many of today's steppers use 248 nm deep ultraviolet (DUV) light to image wafers. 193 nm and 157 nm systems are in development and will further decrease minimum printable line widths. 15 nm extreme ultraviolet (EUV) and x-ray lithography technologies offer potential for decreasing line widths to even smaller dimensions, but these techniques present significant technical challenges and prohibitive cost. Materials that are transparent to DUV light are opaque in the EUV and x-ray regions, so these new technologies will have to develop expensive new optics technologies. Furthermore, EUV and x-ray sources with sufficient intensity to print images are rare and expensive. The technical challenge and cost of implementing EUV and x-ray lithography technologies clearly warrant the investigation of other pattern transfer technologies for use in the semiconductor and micro-machining industries.

1.2 Imprint Lithography

Imprint lithography offers an alternative high-resolution pattern transfer technology. In this process, a template is pressed into a thermoplastic. The polymer conforms to a relief image of a circuit in the template. As this approach uses no optics, diffraction does not limit minimum printable line widths. The topography of the imprint template defines the pattern transferred to the silicon

wafer. A typical imprint lithography is described next. Professor Chou, et. al., at Princeton have studied various versions of this process for micro-machining and lithography applications.

1.2.1 Imprint Lithography Process Description

Figure 1.2 illustrates a typical imprint lithography process. To begin the process, a wafer is spin-coated with a thermoplastic and a transfer layer. The thermoplastic is heated to its glass transition temperature so that it can flow, and a template is then pressed into the pliable thermoplastic. Once the thermoplastic has conformed to the shape of the template, the assembly is cooled, and the wafer and template are separated. The image in the thermoplastic is then copied into the transfer layer and the wafer via chemical etch processes.

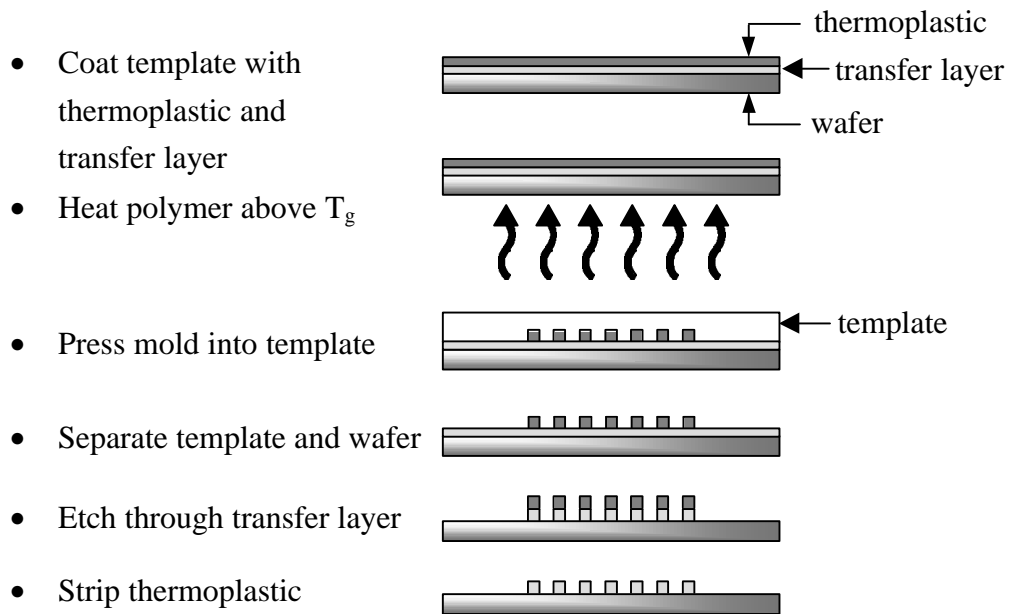


Figure 1.2 Imprint lithography process

1.2.2 Technical Challenges

Imprint lithography faces two distinct challenges: overlay and image transfer fidelity. High temperatures and pressures during the image transfer process distort the template and wafer. Quartz and polysilicon have coefficients of thermal expansion of $4.8 \times 10^{-7} \text{ }^\circ\text{C}^{-1}$ and $4.2 \times 10^{-6} \text{ }^\circ\text{C}^{-1}$ respectively. A temperature change of $300 \text{ }^\circ\text{C}$ would cause a 25 mm quartz template to elongate 3.66 microns. A 75 mm diameter silicon wafer would suffer a 96 micron change in dimension. Pressures on the order of hundreds of psi would cause similarly large distortions in the wafer and template. Such changes in dimension are clearly unacceptable when printing sub-100 nm features.

Such dimensional instabilities make it extremely difficult if not impossible to overlay multiple layers of an integrated circuit. An overlay scheme for such a system would have to account for thermal and mechanical distortions in the template and wafer. It is important to note that these distortions will depend on the process parameters (i.e. temperature and pressure) of every step of the image transfer process. The overlay process will have to be altered every time a process parameter is altered. While technology and engineering ingenuity may overcome these obstacles, they will increase the complexity and cost of imprint lithography and decrease its throughput.

The fidelity of images created with imprint lithography also suffers a pattern density dependence. As a template is pressed into the heated thermoplastic, it must displace significant amounts of material. Figure 1.3 illustrates three patterns to be transferred via imprint lithography. Isolated features that displace little material present little challenge to the imprint lithography process. Gratings and features that displace moderate amounts of thermoplastic present significant challenges to the imprint process. Isolated trenches present an extreme challenge to this process. Any material that does not

fill the trench must be displaced to the side of the template. Image fidelity suffers when patterns incorporate numerous isolated trenches.

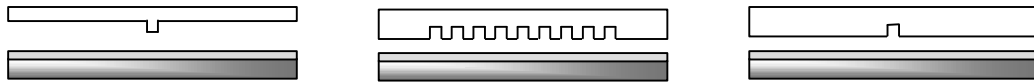


Figure 1.3 Imprint lithography pattern density dependence

(from left to right) a) isolated line b) grating structure c) isolated trench.

This pattern density dependence is especially apparent when printing isolated trenches or large features. These shortcomings have lead researchers at The University of Texas at Austin to pursue an alternative lithography scheme known as Step and Flash Imprint Lithography.

1.3 Step and Flash Imprint Lithography

Step and Flash Imprint Lithography (SFIL) offers another means to transfer images with high resolution, high fidelity, and high throughput. SFIL uses chemical and mechanical processes to transfer images at room temperature with minimal force. The topography of a master template defines the pattern transferred to the wafer, and no projection optics are used.

1.3.1 Template Generation

SFIL is a pattern transfer process and requires a master template. Initial templates have been fabricated via a process very similar to the one used to manufacture phase shift masks. A quartz photomask blank is coated with chromium and a photoresist. The photoresist is patterned with a direct write electron beam machine, and the pattern is transferred to the chromium. At this point, the template is essentially a traditional photomask used in optical lithography. Next, the chromium is used as an etch barrier and the circuit pattern

is etched into the quartz. The chromium is then stripped off the quartz. The end product of this process is a quartz template bearing a relief image of the circuit pattern.

1.3.2 Step and Flash Lithography Process Description

SFIL could probably best be described as a micro-molding process. A master template bearing a relief image defines the pattern to be transferred. SFIL and traditional imprint lithography are similar in the fact that they both use the topography of a template to define the pattern created on the substrate. No projection optics are involved. The key difference between SFIL and traditional imprint lithography is the use of a liquid etch barrier to create a low aspect ratio pattern much like the 2P process developed at Phillips [Haisma, 1996]. This low viscosity solution eliminates traditional imprint lithography's need of high temperatures and pressures. Once low aspect ratio features have been created in the etch barrier, they are copied to a transfer layer using a chemical etch process.

Figure 1.4 illustrates the SFIL process. SFIL uses two organic films to transfer images from a template to a silicon substrate. This process is similar to conventional bilayer schemes used in optical lithography processes today. To begin the process, an organic transfer layer is spin-coated on a silicon substrate. This organic transfer layer will eventually serve as a sacrificial masking layer when processing the substrate. In preliminary trials, negative photoresist have been used as a transfer layer.

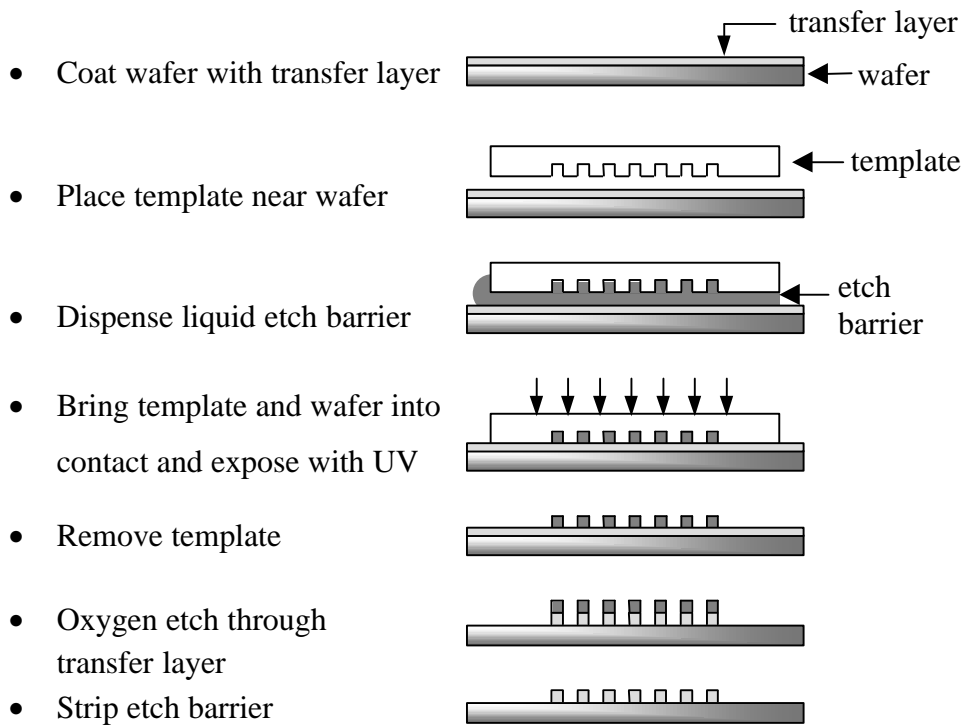


Figure 1.4 Step and flash imprint lithography process

In the next step of the process, a quartz template bearing the relief image of a circuit is brought into the proximity of the coated silicon substrate. Once the substrate and template have been brought into proximity, a drop of a low viscosity photopolymerizable, organosilicon etch barrier is dispensed. The liquid then fills the gap between the template and wafer via capillary action [Colburn, 1999]. The use of a liquid etch barrier gives SFIL its main advantage over traditional imprint lithography. By shaping a liquid instead of a highly viscous thermoplastic, SFIL trades the process control parameters of temperature and pressure for material properties. Developing a SFIL process requires optimization of the chemistry of the etch barrier, transfer layer, and template surface treatment much more than temperature and pressure. The lack of varying temperatures and pressures makes

SFIL much more compatible with mechanical alignment and orientation schemes than traditional imprint lithography.

Once the liquid etch barrier fills the gap via capillary action the template and wafer are pressed together. The etch barrier is then irradiated with ultraviolet light through the top side of the template. A blanket ultraviolet exposure cures the photopolymer and creates a solidified, silicon rich, low surface energy film in the shape of the circuit image on the template. It is important to note that the ultraviolet light does not pattern the etch barrier; it simply initiates crosslinking in the polymer. SFIL uses no projection optics. The patterned template defines the image transferred to the etch barrier.

Once the photocuring is complete, the template is separated from the substrate leaving a patterned, cross-linked, silicon containing etch barrier. After the template and substrate are separated, the pattern in the etch barrier is etched into the transfer layer. At this point in the process, the silicon substrate is coated with a sacrificial imaging layer analogous to the imaged substrate created after the first etch of an optical lithography bilayer process. An oxygen reactive ion etch may then be used to transfer a high aspect ratio image to the silicon wafer.

1.3.3 Technical Challenges

Researchers developing SFIL face a number of chemical and mechanical challenges. Materials research concentrates on the development of appropriate etch barrier, transfer layer, and template treatment chemistries. The surface energies of the transfer layer, etch barrier, and template are tuned to draw the liquid etch barrier into the gap between the template and substrate. To insure image fidelity, the etch barrier must wet all of the surfaces of the template. Bubbles or voids in the etch barrier will generate defects in later steps of the pattern transfer process.

In addition to wetting the template, the etch barrier must also release from the template once it cures. Surface energies of the etch barrier, template, and transfer layer are tuned such that the cured etch barrier adheres to the transfer layer and not to the template. A significant portion of the work on this project has focused on developing materials with surface energies and surface tensions that meet these requirements. Other research focuses on improving the rate of polymerization of the etch barrier and identifying etch processes to transfer patterns from layer to layer.

Another aspect of the research program deals with the design of a machine to implement Step and Flash Imprint Lithography. Such a machine must hold a template and a silicon wafer. It must bring them into contact, dispense an etch barrier solution, and irradiate this structure with ultraviolet light. A focal point of the machine development deals with the interaction of the template and wafer. The template and wafer must be in parallel contact when irradiated with ultraviolet light.

The remainder of this document focuses on the design of a prototype lithographic press used for initial development studies of SFIL. A passive selectively compliant stage is developed to obtain large-area contact between a wafer and a template. This machine allows researchers to investigate the resolution capability of the SFIL process and develop etch barrier and transfer layer materials. Future studies will investigate active stages and nanometer resolution optical sensing schemes to further investigate the template-wafer interface.

2 Imprint Machine Design

A significant portion of SFIL development work has focused on the design and construction of a lithographic press to implement the SFIL process. Initial resolution and SFIL process studies required a machine to transfer an image from a one square inch template to the center of a three inch diameter silicon wafer. This machine enabled testing of various etch barriers, transfer layers, and template surface treatments. This machine was also used for many of the first SFIL image transfer trials.

Such a machine must perform many functions. It must hold the wafer and template with minimal distortion and damage. It must also bring the wafer and template into parallel contact. Such a machine must illuminate the template and wafer with UV light and measure the force required to separate the template and wafer after curing. Since the machine is used in a research environment, it must be reasonably simple to modify, and it must allow the user access to the template and wafer during processing.

Figure 2.1 shows a side view of the SFIL press prototype. To transfer an image, one first mounts a template in the template seat and places a silicon wafer on the orientation stage. The template seat and orientation stage lie inside a press constructed of two horizontal plates and four 24 mm diameter linear roller bearings constructed by Agathon, Inc. The roller bearings are preloaded to only allow vertical motion between the template and the wafer. This vertical motion protects transferred features by minimizing lateral motions between the template and wafer.

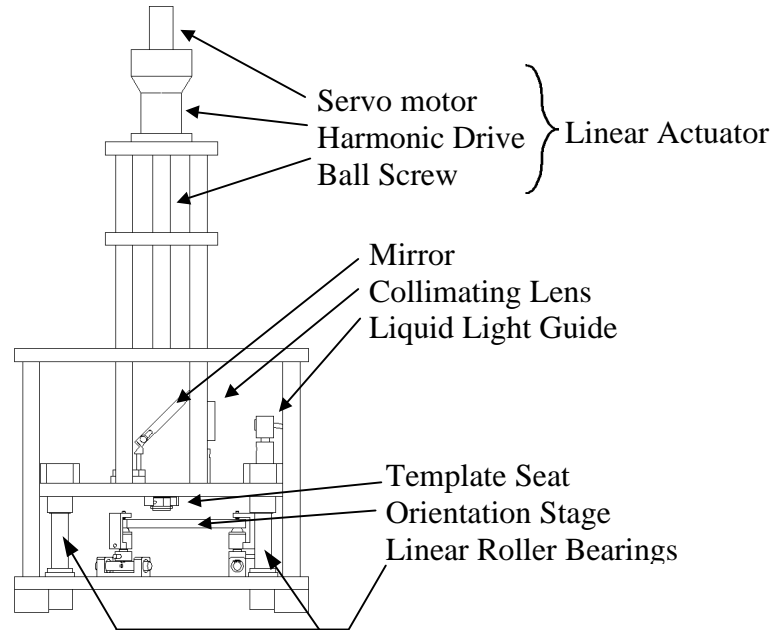


Figure 2.1 Step and flash press

A linear actuator consisting of a Reliance Electric rotary Brushless DC motor (model #1843622004), a 1:160 gearhead from Harmonic Drive Technologies, and a Thomson Saginaw 0.631 diameter 0.2 pitch precision ground ball screw then slowly lowers the template until it rests directly above the silicon wafer. The resolution, R , of the actuator may be calculated by examining the encoder on the servomotor, the ratio of the harmonic drive, and the pitch of the ball screw:

$$R = \frac{1 \text{ motor rev}}{2000 \text{ counts}} \times \frac{1 \text{ HD rev}}{160 \text{ motor rev}} \times \frac{0.2 \text{ inches}}{1 \text{ revolution}} \times \frac{25400 \text{ microns}}{1 \text{ inch}} = \frac{0.02 \text{ microns}}{\text{count}}$$

The use of a preloaded ball screw nut and harmonic drive minimize backlash. Other factors such as compliance of the harmonic drive, motor feedback errors, ball screw machining errors and thermal drift reduce the accuracy of the system to the order of tens of microns. The length of the ball screw allows the template seat to travel almost six inches from its lowest position to its highest position. This allows for easy installation of any future orientation stage designs and lets researchers raise the template to inspect or modify a template or wafer during a printing process.

Once the template rests directly above the wafer, an ultraviolet curable etch barrier is dispensed and fills the gap between the template and the wafer via capillary action. After the etch barrier fills the gap between the template and wafer, the linear actuator presses the template onto the wafer. The wafer is mounted on a compliant orientation stage that flexes to allow the wafer to match the orientation of the template. Chapter 3 discusses the orientation stage in greater detail.

A tripod arrangement of three force sensors below the orientation stage senses when the template and wafer make contact. After the template and wafer are pressed together, ultraviolet light illuminates the etch barrier. An Oriel mercury vapor lamp provides UV light with a peak near 365 nm. A liquid light guide directs the light into the machine. A lens collimates the light exiting the liquid guide and a mirror reflects the light onto the template-wafer interface. After the etch barrier is cross-linked, the linear actuator separates the template and wafer. The template and wafer may then be removed from the machine for inspection and further processing.

3 Orientation Stage Development

Once the frame of the SFIL machine was constructed, the focus of the mechanical design process shifted to a wafer orientation stage. To transfer high-resolution features with high fidelity, it is essential that the template and wafer be in parallel contact. Figure 3.1 illustrates an angular misalignment α between the template and wafer. Such a misalignment leaves a wedge shaped etch barrier after the template and wafer have been separated. The etch processes used to transfer the image in the etch barrier to the transfer layer require a thin uniform etch barrier. The pattern on a wedge shaped etch barrier such as the one shown in Figure 3.1 cannot be etched into the transfer layer. A wafer orientation stage must correct these angular misalignments.

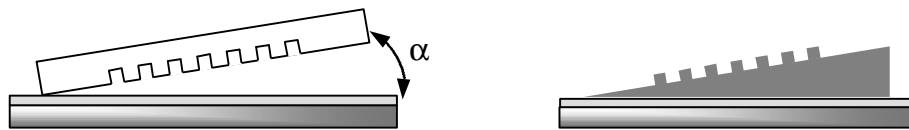


Figure 3.1 Angular misalignment between template and mask

While the stage must correct for angular misalignment, it must also minimize lateral motions that might damage transferred features. If the template and wafer were to slide across one another after the etch barrier is cured, features in the etch barrier could be damaged or sheared off. Thus, any SFIL machine must correct angular misalignments between the template and wafer and minimize lateral or shear motions between the two surfaces.

Figure 3.2 illustrates desired and undesired motions between the template and wafer. Matching the wafer's orientation with the orientation of the template

requires α and β rotations and translation in the z direction. To minimize lateral motions between the template and wafer, one should avoid translations in x and y and γ rotations.

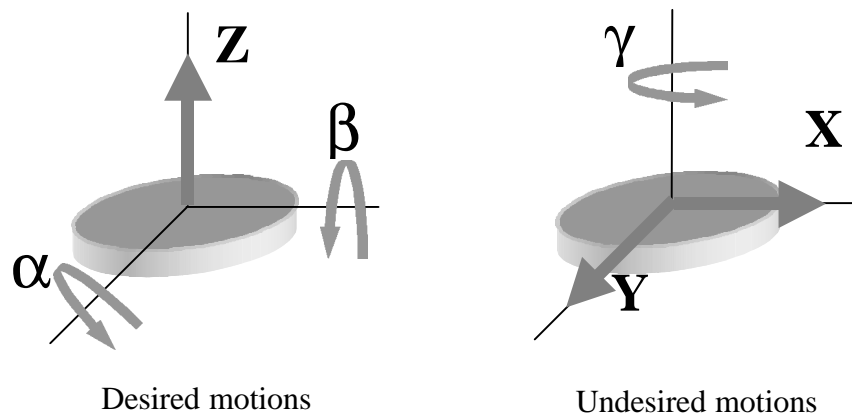


Figure 3.2 Desired and undesired motions between template and wafer

The first SFIL prototype press uses a passive compliant wafer orientation stage to meet these kinematic requirements. The basic challenge in developing the wafer orientation stage was to design a stage with selective compliance. The stage should allow α and β rotations and z translation while minimizing x and y translations and γ rotations. A passive stage that allows only these motions provides a simple, repeatable, and compact solution to the wafer template orientation misalignment problem. The following sections describe the design evolution of the first wafer orientation stage.

3.1 Introduction to Screw System Theory

Screw system theory (SST) provides a useful tool for examining the kinematics of rigid bodies in three dimensions. Sections 3.1.1 through 3.1.4 present a summary of screw system theory extracted from Choi, 1998. Screw system theory has been known to provide a geometric approach to the description

of velocity and force systems associated with systems of rigid bodies. Therefore SST provides geometric insights which may be obscured by the complex nature of the analytical models of spatial mechanisms and robotic systems.

3.1.1 Screw axis (\$)

A screw is a pure geometric concept which is comprised of a line in space (screw axis) along with pitch. A screw can be used to denote both spatial velocity and force systems associated with a rigid body. The concept of a screw is now developed using the velocity state of a rigid body. The instantaneous motion of a rigid body moving freely in space can be fully described by six velocity components: three rotation and three translation velocities. A screw axis is defined such that all points in the body (or extension of the body) that lie on the instantaneous screw axis have the same velocity along the screw axis. Such a screw axis always exists for spatial motion except in the case of pure translation. This axis is also unique if it exists

The motion of the rigid body can be described using the rotation and translation velocities about and along the screw axis respectively. A point of the rigid body that does not lie on the axis moves along the helix of Figure 3.3.

The velocity of this point can be divided into two components. One of these components, v_s , is parallel to the screw axis. This component is the same for all points in the rigid body. Figure 3.3 shows the geometry of the velocity field.

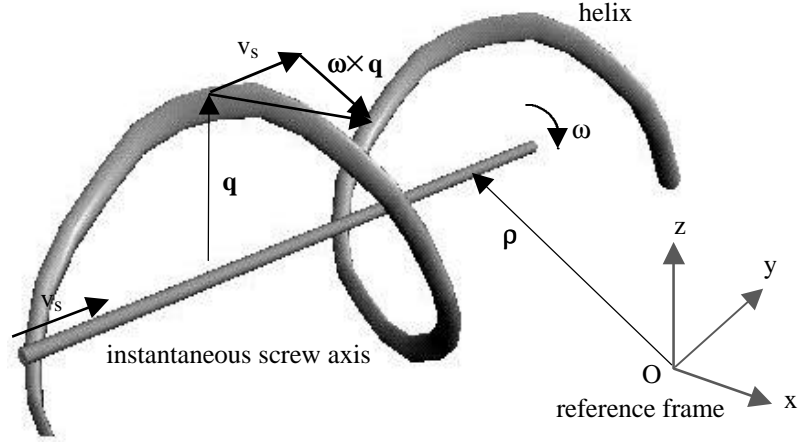


Figure 3.3 The geometry of the velocity field of points in a rigid body

A general single-degree of freedom screw is represented by a 6×1 vector,

$$\mathcal{S} = \begin{pmatrix} \mathbf{w} \\ (h\mathbf{w} - \mathbf{w} \times \boldsymbol{\rho}) \end{pmatrix} = \begin{pmatrix} \mathbf{w} \\ \lambda \end{pmatrix} \quad (3.1)$$

where \mathbf{w} is the screw axis direction, h is the pitch of the screw and $\boldsymbol{\rho}$ is the position vector of any point on the screw axis with respect to the origin of the reference frame. The pitch of the screw (h) can be computed as $h = \mathbf{w} \cdot \boldsymbol{\lambda}$. As an example, a revolute joint is a screw with zero pitch and is given by

$$\mathcal{S} = \begin{pmatrix} \mathbf{w} \\ -(\mathbf{w} \times \boldsymbol{\rho}) \end{pmatrix} \quad (3.2)$$

and prismatic joint, which is an infinite pitch screw, is given by $\mathcal{S} = (\mathbf{0}^T \mathbf{d}^T)^T$, where \mathbf{d} is the unit vector directed along the prismatic axis direction. The instantaneous motion potential of joints with multiple degrees of freedom (m DOF) are represented by $6 \times m$ matrices whose columns are individual screws.

3.1.2 Motor ($\hat{\mathbf{v}}$)

While a screw is a purely geometric quantity, a motor is the representation of spatial velocity of a rigid body. It can be obtained by multiplying the scalar angular velocity about the screw axis with the screw vector. A motor about a screw axis is a 6×1 vector and is represented by a pair of 3×1 vectors. The top vector, referred to as $\boldsymbol{\omega}$, is the angular velocity of motion about the screw axis. The direction of the angular velocity is parallel to the screw axis. The lower vector, referred to as $\boldsymbol{\mu}$, is the linear velocity, produced by the screw motion about the axis with angular velocity $\boldsymbol{\omega}$, of the point in the rigid body which instantaneously coincides with the origin of the reference frame: $\hat{\mathbf{v}} = (\boldsymbol{\omega}^T \boldsymbol{\mu}^T)^T = \boldsymbol{\omega} \boldsymbol{\mu}$. In the case of a prismatic joint, $\boldsymbol{\omega} = \mathbf{0}$ and $\boldsymbol{\mu} = \boldsymbol{\mu} \mathbf{d}$.

3.1.3 Wrench ($\hat{\mathbf{f}}$)

The geometric concept of screw is now extended to represent force systems. A wrench, about a screw axis is a 6×1 vector and is represented by a vector pair $(\mathbf{F}^T, \boldsymbol{\tau}^T)^T$ where \mathbf{F} is the resultant force of the force system represented by the wrench and $\boldsymbol{\tau}$ is the corresponding resultant torque about the origin of the reference frame.

3.1.4 Reciprocity

When two screws, $\$1$ and $\$2$, satisfy the following condition, they are said to be *reciprocal* to each other.

$$(\$1)^T \boldsymbol{\Pi} \$2 = 0 \quad (3.3)$$

where, $\boldsymbol{\Pi} = \begin{bmatrix} \mathbf{0}_3 & \mathbf{I}_3 \\ \mathbf{I}_3 & \mathbf{0}_3 \end{bmatrix}$ and $\mathbf{I}_3 = 3 \times 3$ identity matrix. Between a motor and a wrench system, this is the condition for the wrench to do no work if applied to a

body free to move about the screw axis of the motor [Hunt, 1990]. It should be noted that Equation 3.3 is valid only between two screws one of which is a motor and the other is a wrench. In fact the scalar product defined in Equation 3.3 is not an inner product since it is possible to find non-zero, self-reciprocal screws (a three dimensional pure force (no moment) applied through the center of a ball joint represent a self-reciprocal situation).

Figure 3.4 shows a rigid body connected to the ground by a ball joint and two intersecting revolute joints. When the line of action of the wrench $\hat{\mathbf{f}}$ passes through the intersecting point P and the center of the ball joint, the effect of $\hat{\mathbf{f}}$ passes passively through the serial mechanism to the ground without performing any work on the system. Therefore, the wrench $\hat{\mathbf{f}}$ is reciprocal to the motor representing the motion of the serial mechanism of Figure 3.4.

For a system with m degrees of freedom, there is an instantaneous screw system that is a vector space of order m that characterizes the rate kinematics of the whole system. The reciprocal wrench system is a screw system of order $6-m$.

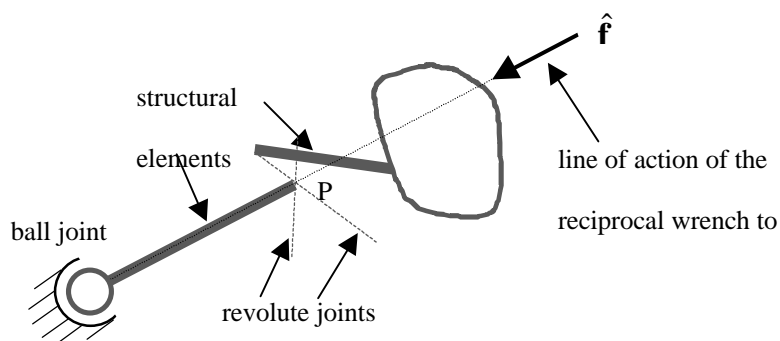


Figure 3.4 A reciprocal wrench, $\hat{\mathbf{f}}$, applied to a body with 5th order motion screw

It is important to note that screw systems are purely geometric quantities. Therefore, the condition for the reciprocity is also purely a geometric relationship.

3.2 First Generation Orientation Stage

A literature search was the first step in developing the orientation stage. Waldron, Raghavan, and Roth present a parallel linkage with three degrees of freedom [Waldron,1989]. Figure 3.5 illustrates this linkage. Two equilateral triangles are separated by three links. Each link consists of a ball joint, a prismatic joint, and a revolute or pin joint. When the triangles are parallel, the system is said to be in its nominal position, and its mobility corresponds to the desired motions of α and β rotations and z translation as shown in the next section.

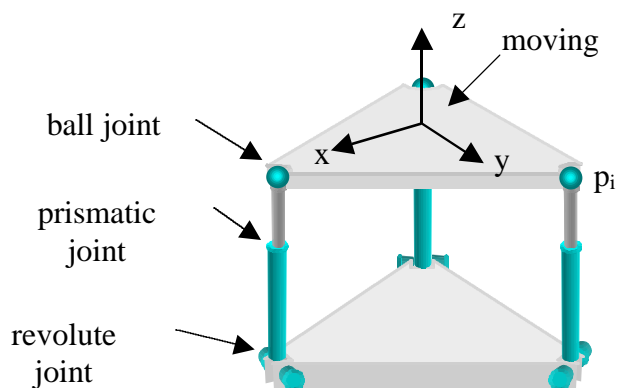


Figure 3.5 Ideal orientation stage kinematic model

3.2.1 Mobility Analysis

To determine the motion capability of this mechanism, it is necessary to find \mathcal{S}_m , the space of motors that describes the stage's motion. This space can be found by looking at the wrenches reciprocal to the mechanism. A reciprocal wrench is a wrench that is transmitted through a linkage to ground without causing the linkage to move. These reciprocal wrenches form a wrench space \mathcal{S}_r .

The motion capability of the linkage is described by the motor space \mathcal{S}_m that is reciprocal to \mathcal{S}_f . Thus, the following procedure may be used to identify \mathcal{S}_m :

1. Identify all wrenches $\hat{\mathbf{f}}_i$ reciprocal to the linkage
2. Identify the space \mathcal{S}_f spanned by all $\hat{\mathbf{f}}_i$
3. Identify the space \mathcal{S}_m that is reciprocal to \mathcal{S}_f

Figure 3.6 illustrates the three wrenches $\hat{\mathbf{f}}_1, \hat{\mathbf{f}}_2$, and $\hat{\mathbf{f}}_3$ that are reciprocal to the initial orientation stage design. Each wrench is reciprocal to one leg of the linkage. Each wrench consists of a pure force that passes through the center of a ball joint. In addition, all of the wrenches lie in the plane formed by the revolute and prismatic joints. Each of these wrenches is transmitted through the linkage without causing the mechanism to move.

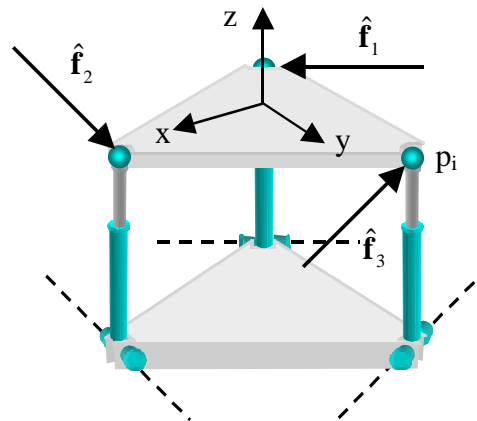


Figure 3.6 Wrenches reciprocal to orientation stage

Since $\hat{\mathbf{f}}_1, \hat{\mathbf{f}}_2$, and $\hat{\mathbf{f}}_3$ lie in the horizontal x - y plane, they can be written in the form $(w_x \ w_y \ 0 \ 0 \ 0 \ \rho w_z)^T$. \mathcal{S}_f is spanned by $\hat{\mathbf{f}}_1, \hat{\mathbf{f}}_2$, and $\hat{\mathbf{f}}_3$. Given \mathcal{S}_f one can calculate \mathcal{S}_m using Equation 3.3.

$$\begin{aligned}
\mathcal{S}_f = \text{span} \left\{ \begin{array}{l} \left(\begin{array}{c} 1 \\ 0 \\ 0 \\ 0 \\ 0 \end{array} \right) \\ \left(\begin{array}{c} 0 \\ 1 \\ 0 \\ 0 \\ 0 \end{array} \right) \\ \left(\begin{array}{c} 0 \\ 0 \\ 0 \\ 0 \\ 1 \end{array} \right) \end{array} \right\} & \begin{array}{l} \text{forces} \\ \text{moments} \end{array} \\
\mathcal{S}_m = \text{span} \left\{ \begin{array}{l} \left(\begin{array}{c} 1 \\ 0 \\ 0 \\ 0 \\ 0 \end{array} \right) \\ \left(\begin{array}{c} 0 \\ 1 \\ 0 \\ 0 \\ 0 \end{array} \right) \\ \left(\begin{array}{c} 0 \\ 0 \\ 0 \\ 0 \\ 1 \end{array} \right) \end{array} \right\} & \begin{array}{l} \text{rotation} \\ \text{translation} \end{array}
\end{aligned}$$

\mathcal{S}_m indicates that the linkage has a mobility of three and can move with three principal motions. These motions are rotation about i and j and translation along k . These are the same α , β and z motions that the orientation stage must have to match the orientations of the template and wafer. Thus, this mechanism provides correct motions for use in a wafer orientation stage.

3.2.2 Detailed Design

Figure 3.7 illustrates a stage design mapped directly from this model. The stage incorporates the same set of joints as the kinematic model: a ball joint, a prismatic joint, and a revolute joint. The ball joint consists of a ball bearing riding in a spherical depression. The ball bearing rests on top of a spring. As a template contacts a wafer placed on top of the stage, the spring supporting the ball bearing deflects and the stage moves. This spring deflection exhibits the same motion as a prismatic joint.

A force transducer in each leg monitors contact forces between the wafer and template. Given the stiffness of the springs supporting the ball bearings, force transducer readings can also be used to calculate stage deflections. The force transducers are mounted on a shaft that acts as a revolute joint. This shaft is mounted in a pair of ball bearings and rotates about its center axis.

Although this stage provides a good starting point for the design process, it needs some improvements. A large number of parts make this design expensive

and difficult to assemble. This high part count also reduces the overall tolerance of the device.

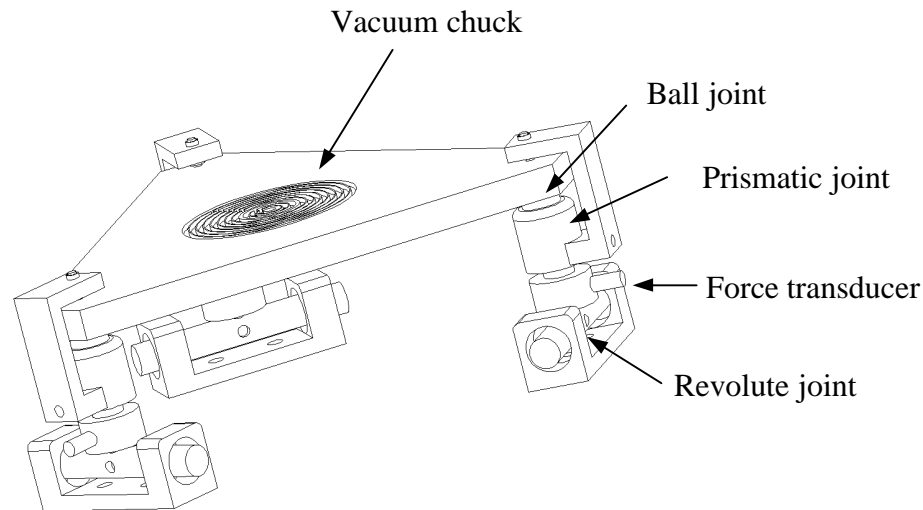


Figure 3.7 Initial wafer orientation stage

Each joint incorporates traditional mechanisms that involve sliding contact. Friction at these sliding interfaces can cause a number of problems with the stage. Particles generated by sliding contact can contaminate the wafer and template and interfere with the imprint process. Friction increases wear on the mechanism and increased clearances decrease the stage's accuracy with time. The stage can also exhibit a phenomena known as stiction that interferes with the stage's performance.

Stiction can be explain by examining the interfaces between two sliding surfaces. In general, the coefficient of static friction between two surfaces is larger than the coefficient of kinetic friction between the same two surfaces. Thus, the force required to start two surfaces sliding over one another is greater than the force required to keep two moving surfaces in motion. This means that joints with sliding surfaces tend to stick before they move. It is difficult to move

sliding joints through small displacements because they tend to move in finite increments between locations where they stick. Problem with stiction, particle generation and wear motivated a search for other orientation stage designs.

3.3 The Use of Flexures in Mechanism Design

Flexures provide a means of eliminating the sliding contact in the joints of the first orientation stage. Flexures avoid sliding contact at joints by replacing parts that slide over each other with parts that bend or flex. Figure 3.8 illustrates a revolute or pin joint and a flexure with similar motions. When the revolute joint undergoes a rotary displacement, the pin slides inside its sheath. Friction due to this sliding motion can generate particles and cause stiction and wear. Particles on the template and wafer can generate defects in the SFIL process. Stiction limits the repeatability and precision of the orientation stage.

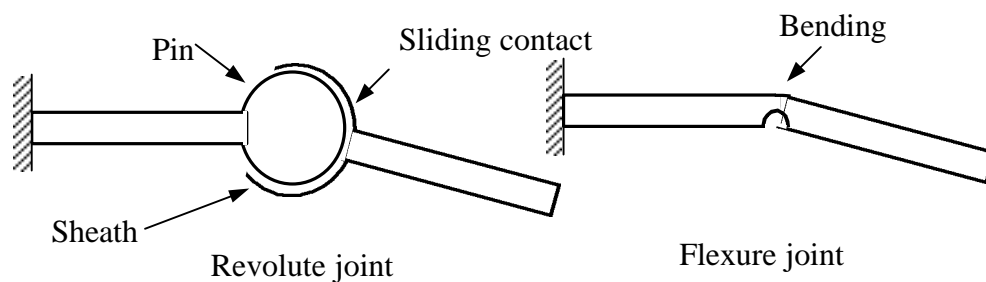


Figure 3.8 Revolute joint and corresponding flexure

Flexures overcome this limitation by avoiding sliding motion between surfaces. When one applies a load to a flexural joint, members in the joint bend or flex instead of sliding over one another. It is much easier to predict and control the linear forces required to move flexures through small displacements. The linear response of flexures makes them more repeatable and easier to move through small displacements.

The absence of sliding contact also increases the lifetime of devices constructed with flexures. Without sliding friction, wear in the mechanism is significantly reduced if not eliminated. One must consider fatigue of flexing joints when predicting a mechanism's service life, but friction and wear effects are minimized.

Flexures exhibit another desirable attribute for high precision equipment. They exhibit no backlash due to clearances. A traditional pin joint such as the one illustrated in Figure 3.8 normally has a slight gap between the pin and the sheath it rests inside. This gap causes a phenomenon known as backlash where, in addition to rotating, the pin moves from side to side inside the sheath. This movement decreases the overall precision and repeatability of the stage.

Roller bearings or ball bearings also offer a means to avoid sliding contact, stiction, and backlash. These devices replace sliding contact with rolling contact. Surfaces in rolling contact experience no sliding friction. Thus, they generate fewer particles and exhibit no stiction effects. Ball and roller bearings may also be preloaded to avoid backlash.

The main difference between flexures and bearings is evident upon an examination of their relative ranges of motion. When flexures are displaced, elements in the joints undergo strain. The range of motion and lifetime of a flexure is most often determined by the amount of strain and fatigue the flexural elements can withstand. Bearings normally have an unlimited range of travel, and their lifetime is usually determined by the wear of elements in contact. A final factor to consider when determining whether to use bearings or flexures is the size of the joint. Small compact linkages often require small compact joints. Bearings consist of many parts and cannot be manufactured as small as flexures. Bearings can significantly increase the size and mass (and thus, reduce the natural frequency) of a linkage. Flexures offer a stiff, lightweight means of

manufacturing joints that are free of stiction, particle generation, and wear due to sliding contact.

3.4 Second Generation Lumped Flexure Stage

A second orientation stage concept uses flexures to avoid problems associated with traditional joints such as backlash, stiction, and particle generation. Such a stage would be more precise and more repeatable than the first orientation stage design. Figure 3.9 illustrates a second generation orientation stage design that uses flexures for all of its joints. The figure on the left illustrates the configuration of five revolute joints r_1 through r_5 in each leg of the stage.

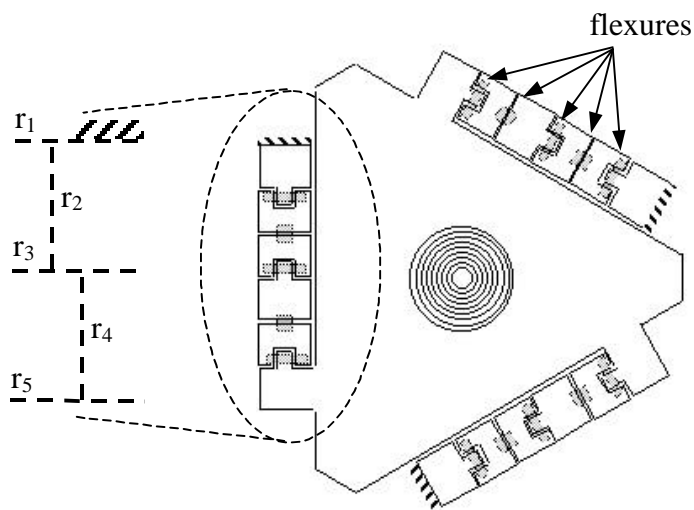


Figure 3.9 Lumped flexure stage

3.4.1 Mobility Analysis

This stage design consists of three legs in parallel. Each leg is a five degree of freedom serial linkage with five revolute flexures. The procedure outlined in Section 3.2.1 may be used to determine the mobility of this

mechanism. Figure 3.10 illustrates three wrenches that are reciprocal to this lumped flexure stage.

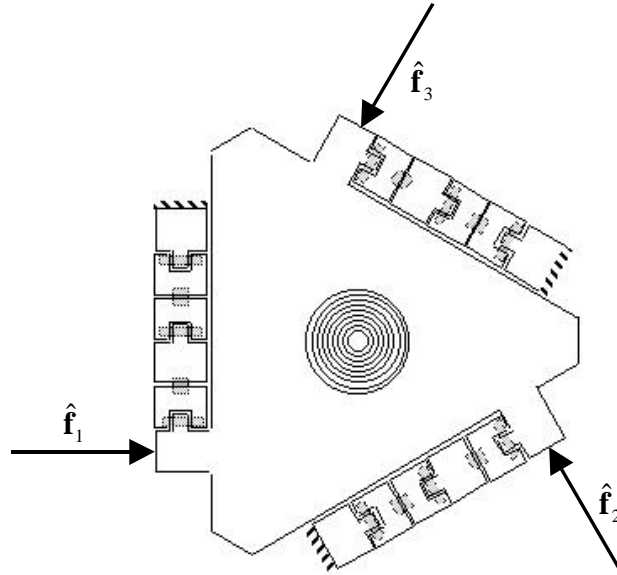


Figure 3.10 Wrenches reciprocal to lumped flexure stage

Any wrench consisting of a force or moment lying in the plane of the stage is reciprocal to the stage. These wrenches may be written in the form $(w_x \ w_y \ 0 \ 0 \ 0 \ \rho w_z)^T$. The reciprocal wrench space \mathcal{S}_f spanned by these wrenches is the same \mathcal{S}_f presented in Section 3.2.1. Thus, the reciprocal wrench space \mathcal{S}_f and the reciprocal motor space \mathcal{S}_m for the lumped flexure stage may be written as

$$\mathcal{S}_f = \text{span} \left\{ \begin{array}{l} \left(\begin{array}{c} 1 \\ 0 \\ 0 \\ 0 \\ 0 \\ 0 \end{array} \right) \\ \left(\begin{array}{c} 0 \\ 1 \\ 0 \\ 0 \\ 0 \\ 0 \end{array} \right) \\ \left(\begin{array}{c} 0 \\ 0 \\ 0 \\ 0 \\ 0 \\ 1 \end{array} \right) \end{array} \right\} \quad \text{and} \quad \mathcal{S}_m = \text{span} \left\{ \begin{array}{l} \left(\begin{array}{c} 1 \\ 0 \\ 0 \\ 0 \\ 0 \\ 0 \end{array} \right) \\ \left(\begin{array}{c} 0 \\ 1 \\ 0 \\ 0 \\ 0 \\ 0 \end{array} \right) \\ \left(\begin{array}{c} 0 \\ 0 \\ 0 \\ 0 \\ 0 \\ 1 \end{array} \right) \end{array} \right\}$$

Again, S_m indicates that the linkage has a mobility of three and can move with three principal motions. These motions are rotation about i and j and translation along k . These are the same α , β and z motions that the orientation stage must have to match the orientations of the template and wafer.

3.4.2 Detailed Design

The lumped flexure stage design incorporates many improvements over the first stage design. As previously mentioned, this stage design eliminates backlash, particle generation, and stiction through the use of flexures. This design also illustrates an alternative geometry that yields the same desired third order mobility as the first orientation stage design. Although the stages have similar numbers of parts, the second stage features a less intricate design and would be simpler to construct and assemble.

However, a few features of the lumped flexure design leave room for improvement. This stage achieves its three degree of freedom mobility by linking three serial arms to one body. Each of the legs uses commercially available revolute flexures. These flexures, however, were too compliant, and the stage design was not stiff enough. When designing highly repeatable and precise mechanisms, one should try to design mechanisms with high stiffnesses and natural frequencies. If a mechanism's fundamental natural frequency is greater than 500 Hertz, the mechanism will be less sensitive to environmental vibrations of frequencies up to 200 Hertz. This design is too compliant and would be very sensitive to environmental vibration.

3.5 Third Generation Distributed Flexure Stage

A third generation orientation stage design provides to improvements based on the lessons learned in the second stage design. Specifically, the design

incorporates the advantages of flexures into a simple compact design with few parts. Further investigation of work in the field of precision engineering produced a mechanism built by Badami, Smith, and Patterson that was used to monitor tilt misalignments with stylus probes [Badami, 1996]. This device uses a flexure ring to achieve three degrees of freedom. Some modifications and adjustments to this design yielded the third wafer orientation stage design. Figure 3.11 illustrates this distributed flexure stage.

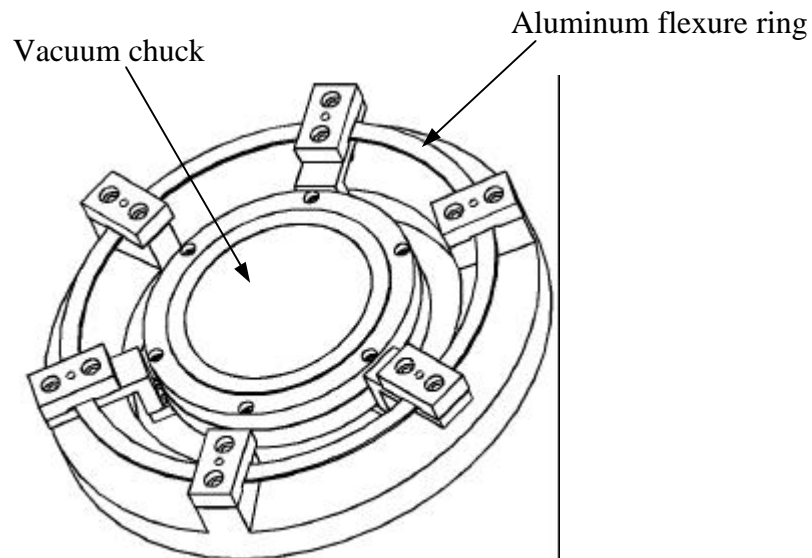


Figure 3.11 Distributed flexure orientation stage

This device derives its motion capability from an aluminum distributed flexure ring. This flexure ring supports a vacuum chuck in the center of the stage. When a template contacts a wafer on the orientation stage, the template generates a moment about the center of the stage. This moment deflects the aluminum ring supporting the vacuum chuck. The circular symmetry of the ring allows the wafer to match the orientation of the template while minimizing lateral motion between the template and wafer.

Beam approximations were used to determine appropriate dimensions for the flexure ring. Each third of the flexure ring was modeled as a straight fixed-fixed beam. Figure 3.12 and Equation 3.4 describes the behavior of a fixed-fixed beam under a load [Gere, 1990].

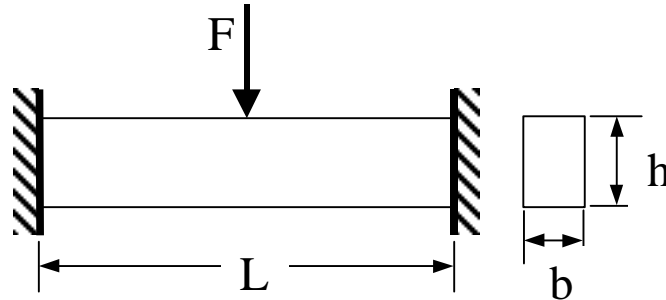


Figure 3.12 Fixed-fixed beam

$$F = \frac{192EI}{L^3} \delta \quad I = \frac{bh^3}{12} \quad (3.4)$$

where

F = force required to deflect beam

E = Young's Modulus of beam material

I = moment of inertia of beam

L = length of beam

b = width of beam

h = height of beam

Equation 3.4 was used to estimate the forces required to deflect a beam. To correct for a few degrees of angular misalignment, the flexure ring is designed so that each segment of the ring deflects roughly 2 mm under a 66 N (15 lb.) load. The ring is made of 7075-T6 aluminum ($E = 72$ GPa). According to Equation

3.4, a 7075-T6 aluminum beam of length $L = 135$ mm, base of $b = 14.5$ mm, and height of $h = 1.27$ mm will deflect 2 mm under a 28 N (6.3 lb) load. The beam can experience four times the stress due to this deflection before it deforms plastically. A flexure ring of these dimensions would deflect roughly 2 mm under an 84 N (18.9 lb) load. The flexure ring incorporated into the distributed flexure stage is based on these dimensions.

This stage design incorporates the advantages of flexures and avoids sliding contact that is present in traditional joints. Its simplistic design uses a small number of parts and can be assembled quickly. This design also presents an interesting kinematic analysis question. There is some question about how to model and analyze the motion capability of a distributed flexure device. Chapter 4 presents a framework for answering these questions and compares the motion capabilities of the ideal three leg kinematic model and the distributed flexure stage.

4 Mobility Analysis

The distributed flexure stage presented in Section 4.3 poses an interesting analysis problem: What is the best way to determine the principal motion capabilities of a mechanism incorporating distributed compliance? Smith and Chetwynd have shown how beam approximations may be used to model individual flexure element [Smith, 1992]. Smith has shown how to approximate the motion of a cantilever flexure as a revolute joint. This chapter presents a system level analysis that looks at a generalized compliance matrix. A finite element model is used to compute the non-ideal compliance matrix of the distributed flexure stage. The results of the finite element model are then used to examine the stage's principal motion capabilities.

4.1 Basis of Comparison

Patterson and Lipkin present a format for investigating the motion capabilities of compliant structures [Patterson, 1993]. A rigid body fully supported by an elastic system has six degrees of freedom. The motion capabilities of the rigid body may be determined by examining the elastic structure supporting the body. For example, the motion capability of the vacuum chuck in the distributed flexure stage may be determined by examining the compliant structure of the aluminum flexure ring. Similarly, the motion capability of the top plate of the ideal kinematic model presented in Section 3.2 may be determined by examining the kinematic structure supporting the plate.

4.1.1 Wrenches, Twists, and the Compliance Matrix

Screw theory offers a means of quantifying the motion capability of a compliant structure. A wrench, $\hat{\mathbf{f}}$, and twist, $\hat{\mathbf{T}}$, may be used to describe the

motion of a rigid body supported by an compliant structure. A wrench in ray coordinates, $\hat{\mathbf{f}} = [\bar{f}^T \quad \bar{\mathbf{t}}^T]^T$, consists of a force, \bar{f} , and a moment, $\bar{\mathbf{t}}$, about a screw axis. A twist in axis coordinates, $\hat{\mathbf{T}} = [\bar{d}^T \quad \bar{\mathbf{g}}^T]^T$ represents a small displacement about a screw axis. \bar{d} represents a linear deflection and $\bar{\mathbf{g}}$ represents a rotational deflection about a screw axis. A compliance matrix \mathbf{C} relates a wrench to a twist:

$$\hat{\mathbf{T}} = \mathbf{C} \hat{\mathbf{f}} \quad (4.1)$$

The Π operator may be used to convert a twist in axis coordinates, $\hat{\mathbf{T}}$, to a twist in ray coordinates, $\hat{\mathbf{t}}$:

$$\Pi \hat{\mathbf{t}} = \hat{\mathbf{T}} \quad (4.2)$$

where

$$\Pi = \begin{pmatrix} 0 & \mathbf{I} \\ \mathbf{I} & 0 \end{pmatrix}$$

Equation 4.1 and Equation 4.2 may be combined to relate $\hat{\mathbf{f}}$ and $\hat{\mathbf{t}}$:

$$\hat{\mathbf{t}} = \Pi \mathbf{C} \hat{\mathbf{f}} \quad (4.3)$$

By assuming that the wrench $\hat{\mathbf{f}}$ and twist $\hat{\mathbf{t}}$ are scalar multiples of the same screw, it is possible to construct an eigenvalue problem:

$$\lambda \mathbf{e} = \Pi \mathbf{C} \mathbf{e} \quad (4.4)$$

This formulation yields six eigenvalues λ_i and six eigenvectors or eigenscrews \mathbf{e}_i . λ_i represents the ratio of angular deformation to force ($\lambda = \gamma / f$). The eigenvectors \mathbf{e}_i are known as eigenscrews in ray coordinates. It is assumed that twists are small displacements about an equilibrium position and that they can

be represented as a vector in \mathbb{R}^6 . A wrench applied about a given eigenscrew \mathbf{e}_i produces a twist about the same eigenscrew \mathbf{e}_i [Patterson, 1993]. Note that Equation 4.4 solves the eigenvalue problem for the matrix $\mathbf{\Pi C}$. The eigenvalues of \mathbf{C} are frame dependent and the resulting eigenvectors do not provide physically meaningful approximation of the motion capabilities of spatial mechanisms.

These eigenscrews of $\mathbf{\Pi C}$ represent the fundamental modes of a compliant mechanism. The eigenscrews represent the directions in which the mechanism can be displaced in a decoupled manner, and the eigenvalues represent the angular deflection about an eigenscrew for an applied wrench. All of the motions of a compliant mechanism may be modeled as linear combinations of the fundamental eigenscrews.

Note that eigenvalues and eigenvectors of the matrix $\mathbf{\Pi C}$ are invariant with respect to the transformation from ray coordinates to axis coordinates. An analysis in ray coordinates yields the same set of eigenvalues and eigenscrews as an analysis in axis coordinates [Patterson, 1993]. Determining the compliance matrix for a partially constrained elastic structure provides a means to examine its motion capability by looking at the eigenscrews of the compliance matrix. For this reason, eigenvalues and eigenscrews provide an attractive tool for comparing the motions of partially constrained compliant mechanisms.

Eigenscrews with zero eigenvalues can be examined to gain some insight into the motion capability of a partially constrained mechanism. The space spanned by all eigenscrews with zero eigenvalues is equal to the space spanned by all wrenches reciprocal to the mechanism. One can find the space spanned by a mechanism's reciprocal wrenches by finding the space spanned by eigenscrews of the $\mathbf{\pi C}$ matrix with eigenvalues equal to zero.

Sections 4.2 and 4.3 compare the motion capabilities of the three leg ideal kinematic model and the distributed flexure stage. Section 4.2 presents an

analytical derivation of the ideal kinematic stage's compliance matrix and its eigenvalues and eigenscrews. Section 4.3 presents the finite element model used to determine the distributed flexure stage's compliance matrix. The eigenscrews and corresponding eigenvalues of the stage are also presented. Section 4.4 compares the motion capabilities of the two mechanisms and presents some a summary of this chapter.

4.2 Ideal Kinematic Stage

This section examines the motion capability of the three leg stage. By treating each of the prismatic joints as a spring with a finite compliance, one can compute the resulting small displacement of the stage about an equilibrium point for a given wrench. This section presents an analytical derivation of the compliance matrix of the three leg kinematic model. The eigenvalues and eigenscrews of the compliance matrix are then examined to provide insight into the model's motion capabilities.

4.2.1 Compliance Matrix

The derivation of the model's compliance matrix begins with an examination of the six screws that span the space of all possible motors of the mechanism. Figure 4.1 illustrates these screws. $\$_1$, $\$_2$, and $\$_3$ represent the motions that the stage can move in. When the stage is loaded, its movement will be a linear combination of motors represented by $\$_1$, $\$_2$, and $\$_3$. $\$_1^r$, $\$_2^r$, and $\$_3^r$ represent the screws reciprocal to the system. A wrench applied along these screws will be transmitted through the linkage and cause no movement.

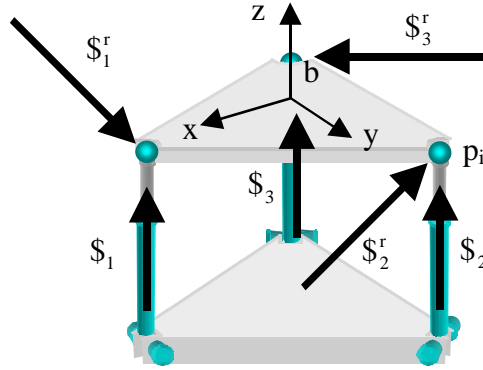


Figure 4.1 Screw representation of three leg model

These six screws can be assembled into an operator that maps a general wrench applied to the system into reciprocal and non-reciprocal components. This operator is known as the Jacobian, \mathbf{J} :

$$\mathbf{J} = [\$_1 \ \$_2 \ \$_3 \ \$_1^r \ \$_2^r \ \$_3^r] \quad (4.5)$$

An applied wrench may be separated into its reciprocal and non-reciprocal components using the Jacobian:

$$\mathbf{J} [f_1 \ f_2 \ f_3 \ f_1^r \ f_2^r \ f_3^r]^T = \mathbf{f}^b \quad (4.6)$$

where \mathbf{f}^b represents a wrench applied to the top surface of the system, $f_1, f_2,$ and f_3 represent forces in the prismatic joints, $f_1^r, f_2^r,$ and f_3^r represent wrenches reciprocal to the linkage.

Motions of the linkage can be examined using these six screws. The velocity of the three corners, $P_1, P_2,$ and P_3 of the top plate, may be related to the velocity of, b , the center of the top plate:

$$V_{P_i} = {}^b \mathbf{m} + {}^b \mathbf{w} \times {}^b p_i \quad (4.7)$$

where

V_{P_i} = velocity of point P

${}^b \mathbf{m}$ = velocity of top plate in frame b

${}^b \mathbf{w}$ = angular velocity of top plate in frame b

p_i = location of point P_i in frame b

By assuming that P_i moves only a small distance along the direction of the screw, the displacement of P_i can be determined:

$$\partial_i = {}^b w_i \cdot ({}^b \mathbf{m} + {}^b \mathbf{w} \times {}^b p_i) \quad (4.8)$$

where

∂_i = small displacement of P_i

${}^b w_i$ = direction vector of Screw $\$i$

Equation 4.8 may be rewritten to express ∂_i in screw notation:

$$\begin{aligned} \partial_i &= [{}^b w_i ({}^b p_i \times {}^b w_i)^T] \begin{pmatrix} {}^b \mathbf{m} \\ {}^b \mathbf{w} \end{pmatrix} \\ \partial_i &= \$i^T \mathbf{p} \begin{pmatrix} {}^b \mathbf{w} \\ {}^b \mathbf{m} \end{pmatrix} \end{aligned} \quad (4.9)$$

The displacements of points P_i along the six screws $\$i$ and $\$i^r$ may be related to the overall twist $\hat{\mathbf{t}}$ of the plate:

$$(\partial_1 \quad \partial_2 \quad \partial_3 \quad \partial_1^r \quad \partial_2^r \quad \partial_3^r)^T = \mathbf{J}^T \mathbf{D} \hat{\mathbf{t}} \quad (4.10)$$

Any displacement ∂_i may be related to the force f_i along a spring via the spring's compliance. The set of six displacements may be related to the set of six spring forces:

$$\Delta \hat{\mathbf{f}} = \hat{\mathbf{t}} \quad \Delta = \begin{pmatrix} 0 & 0 & 0 & 0 & 0 & 0 \\ 0 & 0 & 0 & 0 & 0 & 0 \\ 0 & 0 & 0 & 0 & 0 & 0 \\ 0 & 0 & 0 & c_1 & 0 & 0 \\ 0 & 0 & 0 & 0 & c_2 & 0 \\ 0 & 0 & 0 & 0 & 0 & c_3 \end{pmatrix} \quad \hat{\mathbf{f}} = \begin{pmatrix} f_1 \\ f_2 \\ f_3 \\ f_1^r \\ f_2^r \\ f_3^r \end{pmatrix} \quad \hat{\mathbf{t}} = \begin{pmatrix} \partial_1 \\ \partial_2 \\ \partial_3 \\ \partial_1^r \\ \partial_2^r \\ \partial_3^r \end{pmatrix} \quad (4.11)$$

where Δ includes the effects of compliance of individual joints in the stage. Note that the compliance of the reciprocal springs is represented with a value of zero to denote infinite stiffness in the reciprocal directions.

Substituting Equations 4.6 and 4.10 into Equation 4.11 yields a relationship between an applied wrench and resulting twist:

$$\begin{aligned} \Pi(\mathbf{J}^T \Delta \mathbf{J}^{-1}) \hat{\mathbf{f}} &= \hat{\mathbf{t}} \\ \text{or} & \\ \Pi \mathbf{C} \hat{\mathbf{f}} &= \hat{\mathbf{t}} \end{aligned} \quad (4.12)$$

In Equation 4.12 \mathbf{C} represents the compliance matrix of the structure. One can see from Equation 4.12 that $\mathbf{C} = (\mathbf{J}^T \Delta \mathbf{J}^{-1})$. Appendix A presents calculations to determine \mathbf{C} for the three legged orientation stage. A stage with sides of length equal to one and spring compliances c_i equal to one has the following $\Pi \mathbf{C}$ matrix:

$$\Pi \mathbf{C} = \begin{pmatrix} 0 & 0 & 0 & 2 & 0 & 0 \\ 0 & 0 & 0 & 0 & 2 & 0 \\ 0 & 0 & 0 & 0 & 0 & 0 \\ 0 & 0 & 0 & 0 & 0 & 0 \\ 0 & 0 & 0 & 0 & 0 & 0 \\ 0 & 0 & 0.3333 & 0 & 0 & 0 \end{pmatrix}$$

4.2.2 Eigenscrews and Eigenvalues

The eigenscrews and corresponding eigenvalues for the three leg stage follow directly from the product of $\mathbf{\Pi}$ and the compliance matrix \mathbf{C} . Matrices \mathbf{V} and \mathbf{D} present the eigenscrews and eigenvalues of the matrix $\mathbf{\Pi C}$. Each column of \mathbf{V} corresponds to one eigenscrew of $\mathbf{\Pi C}$. Each diagonal element of \mathbf{D} gives the eigenvalue for the corresponding eigenscrew in \mathbf{V} .

$$\mathbf{V} = \begin{pmatrix} 1 & 0 & 0 & 0 & -1 & 0 \\ 0 & 1 & 0 & 0 & 0 & -1 \\ 0 & 0 & 0 & 0 & 0 & 0 \\ 0 & 0 & 0 & 0 & 0 & 0 \\ 0 & 0 & 0 & 0 & 0 & 0 \\ 0 & 0 & 1 & -1 & 0 & 0 \end{pmatrix}$$

$$\mathbf{D} = \begin{pmatrix} 0 & 0 & 0 & 0 & 0 & 0 \\ 0 & 0 & 0 & 0 & 0 & 0 \\ 0 & 0 & 0 & 0 & 0 & 0 \\ 0 & 0 & 0 & 0 & 0 & 0 \\ 0 & 0 & 0 & 0 & 0 & 0 \\ 0 & 0 & 0 & 0 & 0 & 0 \end{pmatrix}$$

Values presented in \mathbf{V} and \mathbf{D} agree with earlier results in this text. All of the eigenvalues of $\mathbf{\Pi C}$ (diagonal elements of \mathbf{D}) are zero. This indicates that all of the eigenscrews (columns of \mathbf{V}) lie in the reciprocal wrench space \mathcal{S}_r of the mechanism. Each of these eigenscrews can be considered as a wrench that is reciprocal to the mechanism. The first and fifth eigenscrews represent a pure force in the x direction. The second and sixth eigenscrews illustrate a pure force in the y direction. The third and fourth eigenscrews represent a pure moment about z. These wrenches are reciprocal to the ideal kinematic model and will not

cause it to move. The reciprocal wrench space \mathcal{S}_f of dimension three is spanned by these six eigenscrews.

Equation 3.3 provides a means of determining the motor space \mathcal{S}_m that is reciprocal to \mathcal{S}_f :

$$(\mathcal{S}_f)^T \Pi \mathcal{S}_m = 0$$

thus,

$$\mathcal{S}_m = \text{span} \left\{ \begin{array}{l} \begin{pmatrix} 0 \\ 0 \\ 1 \\ 0 \\ 0 \\ 0 \end{pmatrix}, \begin{pmatrix} 0 \\ 0 \\ 0 \\ 1 \\ 0 \\ 0 \end{pmatrix}, \begin{pmatrix} 0 \\ 0 \\ 0 \\ 0 \\ 1 \\ 0 \end{pmatrix} \end{array} \right\}$$

\mathcal{S}_m indicates that the stage can translate in the z direction and rotate about the x and y axes. This analysis agrees with the work presented in Section 3.2.1 that examined the motion capability of the three leg kinematic model. Both analyses found that the ideal model could translate along the z axis and rotate about the x and y axes.

It is interesting to note that the ΠC matrix since its eigenvectors do not span the six-dimensional space [Strang, 1997]. In fact, they only span the three-dimensional reciprocal space. It is well-known in the linear algebra literature that repeated eigenvalues are a pre-requisite for a defective eigenvector space. The eigenvalues of non-ideal stages that have very similar but not identical compliance characteristics as an ideal stage are not likely to be exactly zero. This leads to a case where a near defective matrix possesses six linearly independent eigenvectors. As shown in the following analysis, a careful formulation of the problem is required to allow effective comparisons between ideal and near-ideal stages.

4.3 Distributed Flexure Stage

The distributed flexure stage design presents an interesting analysis problem: given a rigid body supported by an elastic suspension, how is the rigid body's motion capability determined? This section presents a finite element analysis (FEA) of the distributed flexure stage. Data generated from the FEA model is used to determine the structure's compliance matrix. A discussion of the eigenvalue problem for the FEA determined compliance matrix concludes the section.

4.3.1 Finite Element Model

The first step in determining the motion capability of the distributed flexure stage is to compute the stage's compliance matrix. The fact that the distributed flexure stage derives its motion capability from an aluminum flexure ring makes analysis difficult. Traditional methods of computing compliance matrices, such as the one used to determine the compliance matrix of the ideal stage, rely on the geometry of a mechanism and the location of all of its joints. The lack of well-defined joints in the distributed flexure stage makes it difficult to apply these methods. The movement of the flexure would have to be approximated with the movement of individual joints. This process of approximating the flexure's movement quantizes the distributed compliance of the stage and treats it as a group of lumped compliances or joints.

A finite element model provides an alternative means of generating a structure's compliance matrix. Finite element codes allow the user to compute the deflection of a compliant mechanism for a given load. If one knows the deflection of a compliant mechanism for six linearly independent wrenches, one can compute the mechanism's compliance matrix:

$$\mathbf{F} \mathbf{\Pi} \mathbf{C} = \mathbf{T} \quad (4.13)$$

$$\mathbf{\Pi C} = \mathbf{T F}^{-1} \quad (4.14)$$

where

$$\left. \begin{array}{l} \mathbf{F} = 6 \times 6 \text{ matrix of six applied wrenches } \hat{f}_i \\ \mathbf{T} = 6 \times 6 \text{ matrix of corresponding twists } \hat{t}_i \\ \mathbf{C} = 6 \times 6 \text{ compliance matrix} \end{array} \right\} \text{ray coordinates}$$

A finite element model allows a user to model the behavior of a compliant mechanism without having to construct and test the device. Because FEA simulates structures based on the geometry and structure of the entire compliant mechanism, it yields results comparable to those of an actual stage. The comparison of these FEA results to the motions of the ideal model is a key element of this work.

Figure 4.2 illustrates the finite element model used to analyze the distributed flexure stage. IDEAS master series 5.0 software was used to create the finite element model of the distributed flexure stage. Part geometry simulating the flexure ring and vacuum chuck was generated in Pro/Engineer version 20 and exported to IDEAS using an IGES format. The part was then meshed using a free mesh generator in IDEAS. The meshed part contained 817 elements and 2039 nodes.

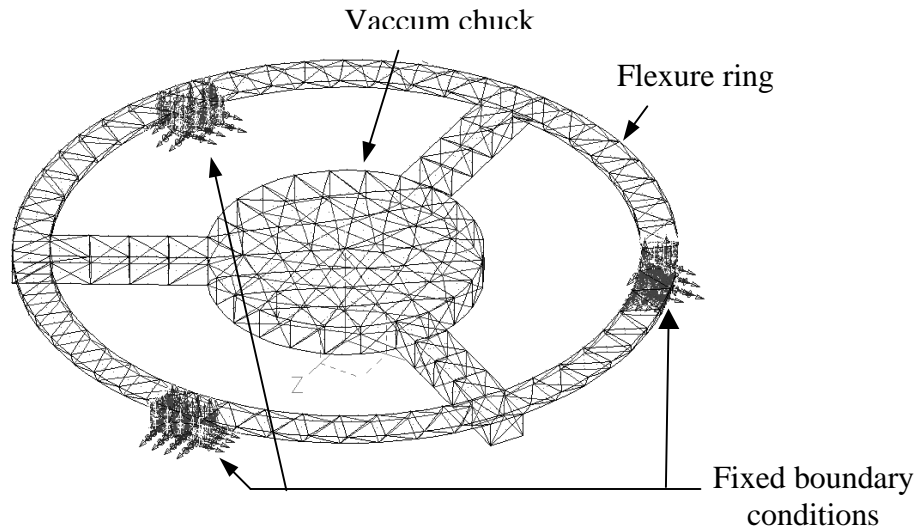


Figure 4.2 Finite element model

Boundary conditions are defined to allow no linear or rotational displacement at the three locations where the flexure ring connects to the base. These conditions simulate a rigid structure supporting the flexure ring.

Six linearly independent wrenches were applied to the structure. Each column of matrix \mathbf{F} represents a wrench applied to the FEA model. The top three elements of every wrench denote linear forces. The lower three elements of every wrench denote moments applied about the center of the vacuum chuck. The first three columns represent forces applied at the center of the vacuum chuck along the x, y, and z axes. The last three columns represent moment generating forces applied at locations other than the center of the vacuum chuck.

$$\mathbf{F} = \left(\begin{array}{cccccc} 66.7 & 0 & 0 & 66.7 & 0 & 0 \\ 0 & -66.7 & 0 & 0 & -66.7 & -66.7 \\ 0 & 0 & 66.7 & 0 & 0 & 0 \\ 0 & 0 & 0 & 0 & 124.1 & 1.7962 \\ 0 & 0 & 0 & -1416.5 & 0 & 0 \\ 0 & 0 & 0 & 0 & -1840.2 & 362.6 \end{array} \right) \left. \begin{array}{l} \text{forces} \\ \text{moments} \end{array} \right\}$$

The finite element model computes a deflection for every individual applied wrench. Figure 4.3 illustrates the finite element model computation of the stage's deflection under a vertical load (second column of \mathbf{F}). The undeformed model is shown as a black wireframe, and the deformed model is shown as a shaded contour plot. Shading indicates von Mises stresses in the structure as it deforms.

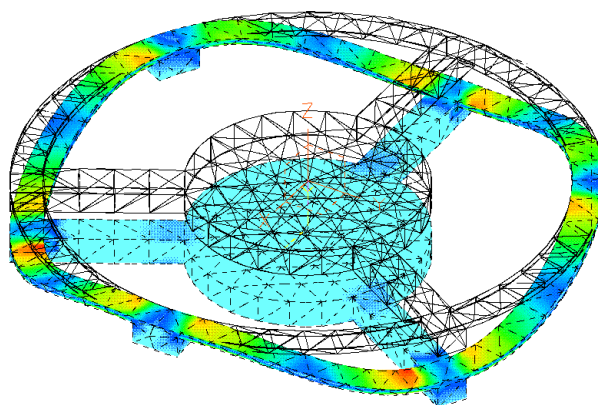


Figure 4.3 Deflected finite element model

The finite element model outputs the deflection of the stage as a set of node deflections. Waldron outlines a method for relating initial and final locations of three points on a rigid body that undergoes a displacement to an equivalent screw displacement [Waldron, 1993]. This method was used to convert the nodal displacements of three points on the vacuum chuck to a corresponding screw displacement. By assuming small displacements, these screws are represented as twist vectors. Appendix B presents a MATLAB file that details these calculations. Matrix \mathbf{T} presents the twists corresponding to each wrench in matrix \mathbf{F} . Each column \mathbf{T} represents the twist due to the wrench represented by the corresponding column of \mathbf{F} .

$$\mathbf{T} = \left(\begin{array}{cccccc} 0 & 0.0016 & 0.0005 & 0 & 0.0023 & 0.0117 \\ 0 & 0 & 0 & -0.0001 & 0 & 0 \\ -0.0005 & 0 & 0 & -0.0005 & -0.0116 & 0.0023 \\ 0.0198 & 0 & 0 & 0.0192 & 0.0225 & -0.0046 \\ 0.0001 & -1.4180 & -0.0013 & 0 & -1.4169 & -1.4549 \\ 0 & 0.0024 & 0.0197 & 0 & 0.0037 & 0.0230 \end{array} \right) \begin{array}{l} \left. \vphantom{\begin{matrix} 0 \\ 0 \\ -0.0005 \\ 0.0198 \end{matrix}} \right\} \text{rotation} \\ \left. \vphantom{\begin{matrix} 0.0001 \\ 0 \end{matrix}} \right\} \text{translation} \end{array}$$

Given matrices \mathbf{T} and \mathbf{F} , one can use Equation 4.14 to compute $\mathbf{\Pi C}$:

$$\mathbf{\Pi C} = \mathbf{T F}^{-1} = \left(\begin{array}{cccccc} 0 & 0 & 0 & 0 & 0 & 0 \\ 0 & 0 & 0 & 0 & 0 & 0 \\ 0 & 0 & 0 & 0 & 0 & 0 \\ 0.0003 & 0 & 0 & 0 & 0 & 0 \\ 0 & 0.0213 & 0 & 0 & 0 & 0 \\ 0 & 0 & 0.0003 & 0 & 0 & 0 \end{array} \right)$$

4.3.2 Analysis of Wrench and Twist Matrices

A cursory investigation of \mathbf{F} and \mathbf{T} presented in the previous section provides some insight to the behavior of the distributed flexure stage. By assuming that the flexure stage experiences small deflections about an equilibrium point, wrenches and twists in \mathbf{F} and \mathbf{T} may be added to each other. \mathbf{F} may be rewritten so that each column represents a wrench or twist about an axis. Each twist (column) of the matrix \mathbf{T}' corresponds to a wrench (column) of the matrix \mathbf{F}' .

$$\mathbf{F}' = \begin{pmatrix} 66.7 & 0 & 0 & 0 & 0 & 0 \\ 0 & -66.7 & 0 & 0 & 0 & 0 \\ 0 & 0 & 66.7 & 0 & 0 & 0 \\ 0 & 0 & 0 & 0 & 124.1 & 1796.2 \\ 0 & 0 & 0 & -1416.5 & 0 & 0 \\ 0 & 0 & 0 & 0 & -1840.2 & 362.6 \end{pmatrix} \begin{matrix} \left. \vphantom{\begin{matrix} 66.7 \\ 0 \\ 0 \\ 0 \\ 0 \\ 0 \end{matrix}} \right\} \text{forces} \\ \left. \vphantom{\begin{matrix} 124.1 \\ 1796.2 \\ -1416.5 \\ -1840.2 \\ 362.6 \end{matrix}} \right\} \text{moments} \end{matrix}$$

$$\mathbf{T}' = \begin{pmatrix} 0 & 0.0016 & 0.0005 & 0 & 0.0007 & 0.0101 \\ 0 & 0 & 0 & -0.0001 & 0 & 0 \\ -0.0005 & 0 & 0 & 0.0000 & -0.0116 & 0.0023 \\ 0.0198 & 0 & 0 & -0.0005 & 0.0225 & -0.0045 \\ 0.0001 & -1.4180 & -0.0013 & 0 & 0.0011 & -0.0369 \\ 0 & 0.0024 & 0.0197 & 0 & 0.0013 & 0.0206 \end{pmatrix} \begin{matrix} \left. \vphantom{\begin{matrix} 0 \\ 0 \\ -0.0005 \\ 0.0198 \\ 0.0001 \\ 0 \end{matrix}} \right\} \text{rotation} \\ \left. \vphantom{\begin{matrix} 0.0016 \\ 0 \\ 0 \\ 0 \\ -1.4180 \\ 0.0024 \end{matrix}} \right\} \text{translation} \end{matrix}$$

\mathbf{F}' represents forces in Newtons and moments in Newton-millimeters (N-mm). \mathbf{T}' represents rotations in radians and translations in millimeters. Figure 4.4 illustrates the coordinate frame used in the analysis of the distributed flexure stage.

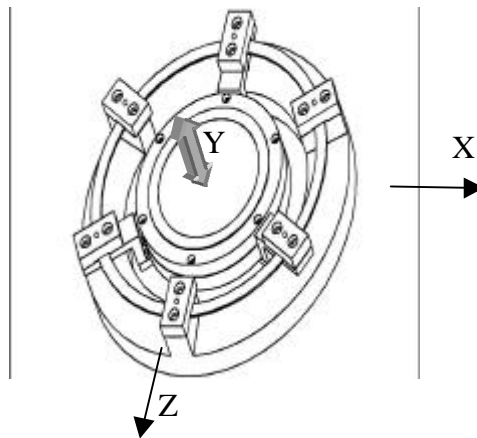


Figure 4.4 Flexure stage coordinate frame

The information contained in \mathbf{F}' and \mathbf{T}' describes the resulting twists \mathbf{t}_i for a set of six linearly independent wrenches \mathbf{f}_i . \mathbf{f}_1 represents a 66.7 N (15 lb.) force applied along the x axis. \mathbf{t}_1 indicates that the stage undergoes a -0.0005 radian (0.03 degree) rotation about the y axis and translates 0.02 mm along the x axis.

\mathbf{f}_2 represents a -66.7 N (-15 lb.) force applied along the y axis. \mathbf{t}_2 indicates that the stage undergoes a 0.0016 radian (0.09 degree) rotation about the x axis and translates 1.4 mm down the y axis.

\mathbf{f}_3 represents a 66.7 N (-15 lb.) force applied along the z axis. \mathbf{t}_3 indicates that the stage undergoes a 0.0005 radian (0.03 degree) rotation about the x axis and translates 0.02 mm along the z axis.

The remaining moment-twist pairs may be interpreted in a similar manner. \mathbf{f}_5 denotes a wrench dominated by a -1840 Nmm moment about the z axis. The corresponding twist \mathbf{t}_5 indicates a -0.0116 radian (0.66 degree) rotation about the z axis and 0.001, 0.02, and 0.001 mm translations along the x, y, and z axes respectively. Thus, a 0.66 degree rotation about the z axis induces a 0.0001 mm translation along the x and z axes.

Note that the stage is compliant about the x and z axes and along the y axis. The stage is most likely to rotate about x and z and translate in z. This initial analysis indicates that the flexure stage's motion capability is very similar to the ideal stage's motion capability. However, these results depend on the coordinate frame used and the applied moments selected. The following section looks for a frame invariant analysis method based on the eigenvalues and eigenvectors of the $\Pi\mathbf{C}$ matrix.

4.3.3 Eigenvalues and Eigenvectors

Given the $\Pi\mathbf{C}$ matrix presented in Section 4.3.1, it is possible to draw some conclusions about the motion capability of the flexure stage. Eigenvectors with

zero eigenvalues identify wrenches that are reciprocal to the mechanism. While this analysis works well for ideal compliance matrices such as the one presented in Section 4.2.1, the eigenvalue analysis of a non-ideal compliance matrix is less straightforward.

Lipkin, et. al. have produced a significant body of work dealing with this eigenvalue problem [Patterson, 1993]. They limit the scope of their work, however, to compliant structures with six degrees of freedom. These unconstrained structures always have eigenvector space of rank six. Constrained compliant structures with fewer than six degrees of freedom have a deficient eigenvector space with a rank less than six. For example, the ideal kinematic model presented earlier in this text is constrained to move with only three degrees of freedom (it has three springs that can deflect). The ideal model has three linearly independent eigenvectors, so the rank of the space spanned by its eigenvectors is three. The ideal stage does not have a complete set of six linearly independent eigenvectors, so it is said to have a deficient eigenvector space.

A deficient eigenvector space by itself does not create a problem with the eigenvalue analysis of a compliance matrix. Difficulties arise, however, if attempts are made to solve the eigenvalue problem for the compliance matrix of a near-ideal stage that has been numerically derived. The finite element model derivation of the distributed flexure stage's compliance matrix is such a case. The flexure stage's compliance matrix is both numerically derived and has a deficient eigenvector space. Solving for the eigenvalues and eigenvectors of \mathbf{PIC} for the distributed flexure stage yields a set of distinct eigenvalues and spurious eigenvectors. These eigenvectors cannot be interpreted to gain insight into a physical system's behavior.

This eigenvalue problem breaks down because the compliance matrix has been numerically computed and it has a deficient eigenvector space. A

compliance matrix with a deficient eigenvector space that is computed directly from geometry, has a set of some zero and some non-zero eigenvalues. Eigenvectors with zero eigenvalues represent wrenches reciprocal to the system. However, since the compliance matrix was numerically computed, one cannot solve for exact eigenvalues. The eigenvalues of the numerically computed compliance matrix are small, but they are not equal to zero. The matrix \mathbf{D} represents the eigenvalues of the $\mathbf{\Pi C}$ matrix of the flexure stage. \mathbf{V} lists the eigenvectors corresponding to the eigenvalues presented in \mathbf{D} .

$$\mathbf{D} = \begin{pmatrix} -4.08 + 0.18i & 0 & 0 & 0 & 0 & 0 \\ 0 & -4.08 - 0.18i & 0 & 0 & 0 & 0 \\ 0 & 0 & 4.08 + 0.17i & 0 & 0 & 0 \\ 0 & 0 & 0 & 4.08 - 0.17i & 0 & 0 \\ 0 & 0 & 0 & 0 & 4.65 & 0 \\ 0 & 0 & 0 & 0 & 0 & -4.65 \end{pmatrix} \quad \text{E-5}$$

$$\mathbf{V} = \begin{pmatrix} 6.187 - 2.893i & 6.187 + 2.893i & -6.011 - 1.981i \\ 0.044 + 0.260i & 0.044 - 0.260i & -0.096 + 0.318i \\ 0.937 - 7.239i & 0.937 + 7.239i & 2.059 + 7.456i \\ -0.102 + 0.076i & -0.102 - 0.076i & -0.105 - 0.057i \\ -0.090 - 0.278i & -0.090 + 0.278i & -0.049 + 0.395i \\ 0.009 + 0.099i & 0.009 - 0.099i & 0.009 + 0.106i \\ -6.011 + 1.981i & -2.863 & -2.709 \\ -0.096 - 0.318i & 9.370 & -9.623 \\ 2.059 - 7.456i & 2.002 & -0.223 \\ -0.105 + 0.057i & 0.031 & -0.042 \\ -0.049 - 0.395i & 9.754 & 10.000 \\ 0.009 - 0.106i & 2.200 & -0.005 \end{pmatrix}$$

Some of the eigenvalues presented in \mathbf{D} have complex values. The eigenvectors in \mathbf{V} are also complex and are not related to the motion capabilities

of the distributed flexure stage. These eigenvectors are of no use in analyzing the flexure stage's motion capability. The following two sections investigate symmetry and scaling as possible causes of this failure of the eigenvalue problem. Section 4.3.3.3 summarizes the results of this investigation of the eigenvalue problem applied to compliance matrices.

4.3.3.1 Symmetry Considerations

Issues of symmetry can arise when one works with compliance matrices and the screw representation of compliant mechanisms. Symmetry refers to the nature of a compliance matrix. Any matrix \mathbf{C} representing the unconstrained compliance of an elastic structure should be real, positive definite, and symmetric. If the elastic structure is partially constrained, the matrix \mathbf{C} is positive semi-definite. In this work, the compliance matrix computed from the results of the finite element model is slightly asymmetric. This asymmetry is most likely due to numerical rounding and nonlinearities in the finite element model. In addition, the screw representation of the FEA model displacement assumes that the central vacuum chuck portion of the FEA model is rigid. Small deflections in this region of the model could contribute to the asymmetry of the compliance matrix.

Examining symmetric and asymmetric components of the compliance matrix provides a means to investigate the impact of this asymmetry. A numerically computed compliance matrix \mathbf{C}_{num} , can be separated into a symmetric component, \mathbf{C}_{sym} , and an asymmetric component of the matrix, \mathbf{C}_{err} .

$$\mathbf{C}_{\text{sym}} = 0.5 * (\mathbf{C}_{\text{num}} + \mathbf{C}_{\text{num}}^T) \quad (4.15)$$

$$\mathbf{C}_{\text{err}} = 0.5 * (\mathbf{C}_{\text{num}} - \mathbf{C}_{\text{num}}^T) \quad (4.16)$$

Solving the eigenvalue problem for $\Pi\mathbf{C}_{\text{sym}}$ yielded the following eigenvalues \mathbf{D} and eigenvectors \mathbf{V} :

$$\mathbf{D} = \begin{pmatrix} 0.4687 & 0 & 0 & 0 & 0 & 0 \\ 0 & -0.3961 & 0 & 0 & 0 & 0 \\ 0 & 0 & -0.4170 & 0 & 0 & 0 \\ 0 & 0 & 0 & 0.3962 & 0 & 0 \\ 0 & 0 & 0 & 0 & 0.4157 & 0 \\ 0 & 0 & 0 & 0 & 0 & -0.4674 \end{pmatrix} \text{E-4}$$

$$\mathbf{V} = \begin{pmatrix} 0.2964 & 0.9995 & 0.0325 & -0.9894 & -0.1260 & -0.0607 \\ -0.4416 & -0.0030 & 0.0235 & -0.0058 & -0.0284 & -0.5381 \\ 0.8469 & 0.0311 & -0.9992 & 0.1448 & -0.9916 & -0.8407 \\ -0.0039 & -0.0290 & 0.0060 & -0.0296 & 0.0026 & 0.0002 \\ -0.8209 & -0.0096 & -0.0480 & 0.0033 & -0.0576 & 1.000 \\ 0.0267 & 0.0059 & 0.0273 & -0.0026 & -0.0278 & 0.0260 \end{pmatrix}$$

It is interesting to note that removing the asymmetric component of \mathbf{C} yielded real eigenvalues of $\Pi\mathbf{C}$. These eigenvalues are distinct; three of them are positive and the others are negative. This is in keeping with the eigenstructure of unconstrained compliant structures as presented by Patterson [1993]. Therefore, due to numerical errors, a partially constrained compliant structure that has six zero eigenvalues and a defective eigenvector space behaves like an unconstrained compliant structure that has a six-dimensional eigenvector space. These eigenvectors of $\Pi\mathbf{C}$, however, still bear no resemblance to the motion capability of the flexure stage.

4.3.3.2 Scaling Considerations

A rigid body that is displaced can experience linear translation and rotation. Thus, a screw, $\$$, describes both rotation and translation. For example, the first three elements of a twist vector represent rotations. The last three elements of a twist represent a linear displacement. Rotational displacements have units of radians, and linear displacements have units of length.

It is possible to break the motion capability of a mechanism down into its fundamental components, this difference in units can complicate an analysis. Solving for the eigenvalues of a compliance matrix is such a case. Units of rotation and units of length must be related in order to decide which motions dominate a mechanism's mobility. For example, consider the matrix \mathbf{T} of twists computed from the FEA model of the flexure stage:

$$\mathbf{T} = \begin{pmatrix} 0 & 0.0016 & 0.0005 & 0 & 0.0023 & 0.0117 \\ 0 & 0 & 0 & -0.0001 & 0 & 0 \\ -0.0005 & 0 & 0 & -0.0005 & -0.0116 & 0.0023 \\ 0.0198 & 0 & 0 & 0.0192 & 0.0225 & -0.0046 \\ 0.0001 & -1.4180 & -0.0013 & 0 & -1.4169 & -1.4549 \\ 0 & 0.0024 & 0.0197 & 0 & 0.0037 & 0.0230 \end{pmatrix} \left. \begin{array}{l} \vphantom{\begin{pmatrix} \\ \\ \\ \\ \\ \end{pmatrix}} \right\} \text{rotation} \\ \left. \begin{array}{l} \vphantom{\begin{pmatrix} \\ \\ \\ \\ \\ \end{pmatrix}} \right\} \text{translation} \end{array} \right.$$

Upon initial inspection, translation may appear to dominate the motions of this mechanism. This assumption, however, is not as easy to make when the units of translation and rotation are examined. In this matrix, rotations have units of radians and translations have units of millimeters. If rotation was quantified in units of microradians, the motion capability of the mechanism would appear to be dominated by rotational motion. This example highlights a fundamental difficulty with spatial motion that combines two fundamentally different kinds of motion:

translation and rotation. The scale of these motions must be considered in order to determine the dominant motions of a body.

4.3.3.3 Summary of the Eigenvalue Problem

While the eigenstructure of a compliant mechanism is a good indicator of its kinematic and load bearing characteristics, its use in comparing the specific stages of Figures 3.7 and 3.11 is limited. The repeated zero eigenvalues and a defective eigenvector space of the ideal stage lead to poorly conditioned numerical approximations of the flexure stage. A robust numerical scheme is therefore required for comparing the ideal and flexure stages. The following section presents such an approach based on strain energy.

4.3.4 The Use of Strain Energy as a Metric

The difficulty of characterizing the behavior of numerically computed non-ideal compliant structures using eigenvalues and eigenvectors illustrates the need for an alternative metric to compare the motion capabilities of compliant spatial mechanisms. The physical quantity of strain energy may be used as such a metric. The amount of work done by a force is the product of a force and the distance through which it acts:

$$W = F d \quad (4.17)$$

where

W = work done by a force F (units of energy)

F = applied force (units of force)

d = the distance through which the force acts (units of length)

The work done by a wrench acting on a compliant structure may be calculated in a similar manner:

$$W = \hat{\mathbf{f}}^T \mathbf{\Pi} \hat{\mathbf{t}} = E \quad (4.18)$$

where

W = work done by wrench (units of energy)

$\hat{\mathbf{f}}$ = wrench applied to structure (units of force, torque)

$\hat{\mathbf{t}}$ = twist representation of structure's deflection (units of length, rotation)

E = strain energy stored in deformed compliant structure (units of energy)

The amount of strain energy stored in a compliant structure is equal to the amount of work an applied wrench performs. In fact, a structure's compliance determines how much strain energy the structure can store in a given configuration. As a wrench deforms an elastic structure, strain energy is stored in compliant members of the structure. Wrenches of the same magnitude applied along stiff portions of an elastic structure will cause little deformation and store little strain energy in the system.

This relationship can be exploited to find wrenches that are “near-reciprocal” to a mechanism. Given an applied wrench and resulting twist, one can calculate the strain energy stored in a compliant structure via Equation 4.18. Wrenches that generate little or no strain energy in the structure are assumed to be near-reciprocal wrenches.

Wrenches and twists computed via the FEA model of the flexure stage confirm this analysis. Table 4.1 lists strain energies calculated from wrenches and twists taken from the FEA model of the flexure stage.

Table 4.1 Strain energy in distributed flexure stage

Strain Energy	Applied wrench
1.3185	15 lb. force along x axis
94.6136	15 lb. force along y axis
1.3125	15 lb. force along z axis
116.1306	10 in-lb. torque about x axis
1.4617	10 in-lb. torque about z axis
119.0054	10 in-lb. torque about y axis

Small strain energies indicate that wrenches consisting of forces along the x and y axes and moments about the z axis are reciprocal to the distributed flexure stage. These three wrenches span the space of wrenches reciprocal to the stage. Wrenches with large strain energies are not reciprocal to the stage. These results confirm that the distributed flexure stage exhibits the motions that are desired in a wafer orientation stage. The flexure stage allows rotations about x and y and translation in z. At the same time, it has low translation in x and y and rotation about z.

4.4 Summary

This chapter examined the ideal stage presented in Section 3.2 and the distributed flexure stage presented in Section 3.5. These two stages were compared to determine the suitability of the distributed flexure stage for use as a wafer orientation stage for imprint lithography. The eigenvalue problem provides a good tool for examining the motion capability of the ideal stage. The distributed flexure stage, however, could only be analyzed using the strain energy metric previously discussed. Both stages exhibit motion characteristics appropriate for use in an imprint lithography orientation stage.

5 Experimental Results

This section presents images of several imprints generated using Step and Flash Imprint Lithography. All results shown in this section were processed using the imprint machine and orientation stage presented in Sections 2 and 3. Images are presented in chronological order according to date of imprint.

5.1 Images on Flat Substrates

Figures 5.1 and 5.2 present atomic force microscope (AFM) images of some of the first SFIL images. Figure 5.1 illustrates a 20 micron gate structure. This image was taken to show that SFIL does not suffer a pattern density dependence and can transfer patterns over large areas. Figure 5.2 presents sub-micron lines and spaces that were used to study the resolution capability of SFIL.

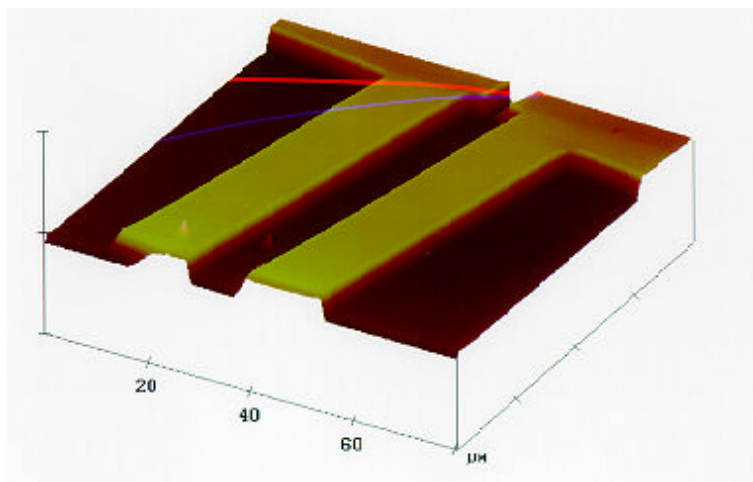


Figure 5.1 AFM image of 20 μm feature

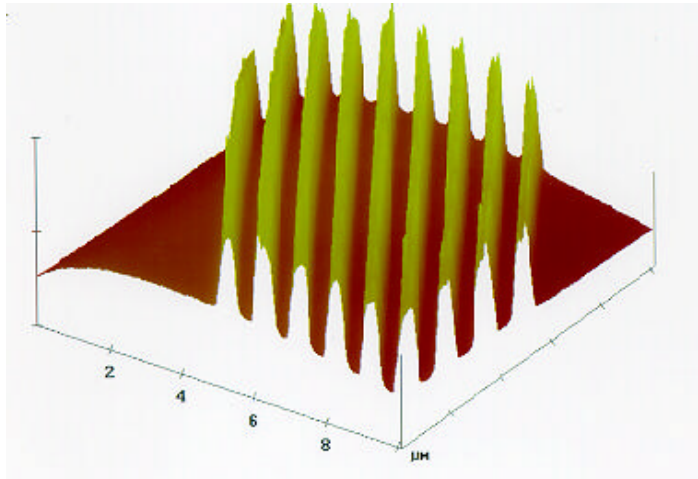


Figure 5.2 AFM image of sub-micron lines and spaces

Figure 5.3 shows 60 nm features on a template (left) and 60 nm features transferred to a silicon wafer (right). It has been observed that SFIL process can replicate sub 100 nm features written on a template. In addition, SFIL can also transfer the minute defects in such small features. Specifically, stitching errors typical of e-beam tools present in the 60 nm template were also replicated onto the wafer. These observations highlight the tremendous resolution capability of the SFIL process.

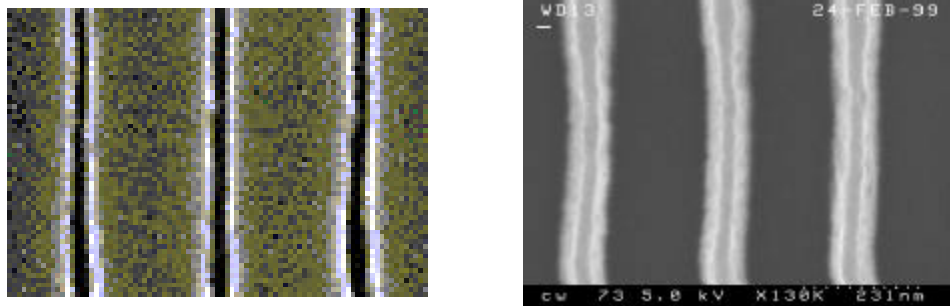


Figure 5.3 60 nm features on template* and etch barrier

* template micrograph courtesy of IBM-Burlington

Figure 5.4 shows a scanning electron microscope (SEM) image of 150 nm etch barrier features transferred from a template written by IBM to wafer surface. This micrograph shows square vertical sidewalls in the patterned etch barrier.

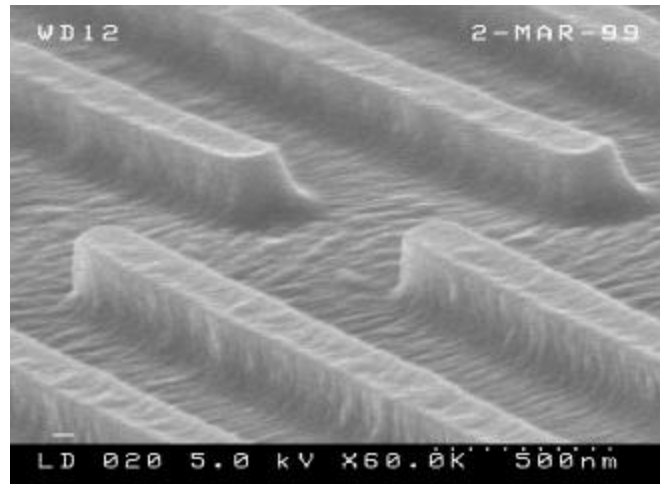


Figure 5.4 150 nm features in etch barrier

5.2 Images on Curved Substrates

Another potential advantage of the SFIL process is its ability to print on curve substrates. An optical lithography technique can in principle be designed to project an image onto special surfaces such as aspheres and cylinders. Even then, the system's projection optics would be specifically designed to project an image onto a single surface. SFIL can transfer patterns from curved templates to curved substrates. Figure 6.3 shows features on template (left) and transferred images on spherical substrate (right). These images were generated using a lens doublet with focal length of 100 mm. The template was attached to a piece of flat square quartz and the substrate was attached to a surface. The template and substrate were then placed in the imprint machine and the pattern was transferred.

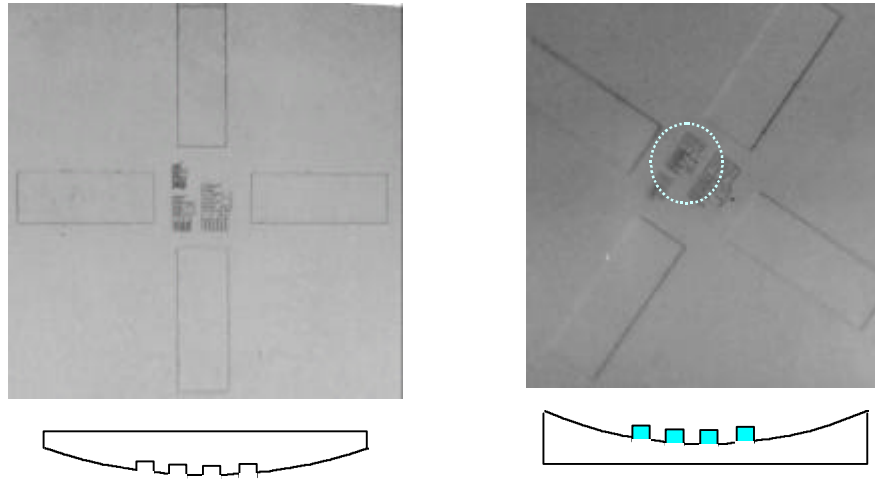


Figure 5.5 Optical micrographs of images on curved template and substrate

Figure 5.6 presents SEM (left) and AFM (right) images of a patterned etch barrier on a curved substrate. A dotted circle in Figure 5.5 indicates the location of these images on the substrate.

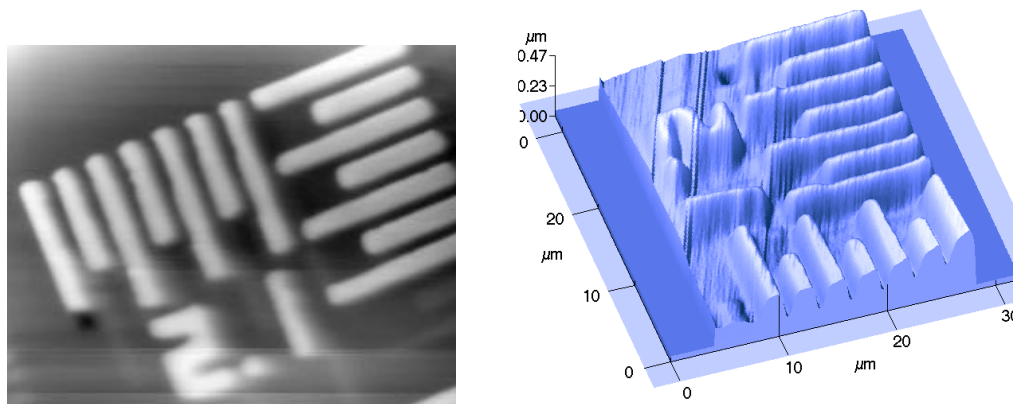


Figure 5.6 SEM and AFM images of patterned spherical substrate

6 Closing Remarks

6.1 Conclusions

Step and Flash Imprint Lithography offers new potential for transferring high-resolution patterns quickly and cost effectively. Research in the areas of machine design and materials development has produced a process that creates sub-100 nm images in an organic etch barrier. SFIL has the potential to decrease both cost and minimum printable feature size by eliminating the use of projection optics.

Significant milestones achieved thus far include the development of functional etch barrier, transfer layer, and template treatment formulations in addition to the design and construction of a prototype imprint machine. Final design and construction of an orientation stage to correct for misalignments between templates and wafers has been completed. These achievements have allowed researchers at The University of Texas at Austin to demonstrate SFIL's sub-100 nm resolution patterning capability on flat and demonstrate SFIL's ability to transfer images to spherical substrates [Colburn, 1999], [Ruchhoeft, 1999].

This work has also presented methods of comparing the motions of spatial mechanisms. The eigenvalues and eigenvectors of a ΠC matrix offer a frame invariant means of comparing the motion capability of ideal stages. Eigenvectors with zero eigenvalues represent wrenches that are reciprocal to a mechanism. However, the eigenvalue problem is very sensitive to numerical rounding errors and nonlinearities. This sensitivity limits the use of the eigenvalue problem to examine the motion capability of non-ideal numerically computed compliance matrices.

Strain energy offers an alternative metric to examine the behavior of compliant structures under load. Wrenches that impart little or no strain energy to

a structure are reciprocal to that structure. The space spanned by these reciprocal wrenches is reciprocal to the space of motors that describes a mechanism's motion capability. The metric of strain energy offers a frame invariant method of comparing the motions of spatially compliant mechanisms and distributed flexures.

6.2 Future Work

The next major milestone in the development of the SFIL process will be to transfer an image in a patterned etch barrier to a silicon substrate. The amount of non-patterned etch barrier remaining after photocuring must be minimized. Researchers currently face a number of questions regarding this task. This section discusses some of these questions and examines other future work in the SFIL project.

6.2.1 Base Layer Thickness

The etch process that will be used to transfer an image in a patterned etch barrier to a silicon substrate requires a minimal or nonexistent residual base layer. Figure 6.1 illustrates a base layer of thickness, t , left after photocuring.

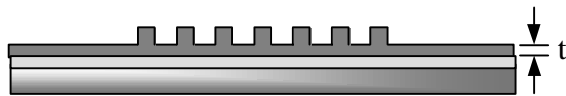


Figure 6.1 Residual base layer

This extra etch barrier material complicates the etch process used to transfer the image in the etch barrier to the transfer layer. To maintain image fidelity during the etch process, the thickness of the residual base layer should be less than the height of the features printed in the etch barrier. Most of the templates used thus far in the SFIL development process have a feature depth of

100 to 200 nm. Currently, researches are attempting to reduce the thickness of the base layer to less than 100 nm.

This problem can be attacked from two directions: dispensing just enough fluid to wet the surfaces and removing any excess liquid. The manner in which the liquid etch barrier is dispensed seems to affect the amount of residual etch barrier left behind. Simply placing a drop of the etch barrier on the wafer and pressing the template onto the wafer leaves base layers 10 microns thick and thicker. Filling the gap between the template and wafer has produced base layer thicknesses on the order of one micron. Spin coating the etch barrier on the wafer before printing may further minimize residual base layer thicknesses, but this method is difficult to implement. It is difficult to keep a spin coated wafer clean when transporting it from the spinner to the imprint machine. One should also note that etch barriers are solutions of compounds of differing weights. Spin coating may push heavier elements towards the edge of the wafer and leave a non uniform etch barrier on the wafer.

The amount of liquid etch barrier dispensed may also be related to the thickness of the base layer. One should dispense just enough liquid to wet the template-wafer interface and fill all of the voids of the template. Any excess liquid not expelled to the edge of the template before photocuring will contribute to the residual base layer.

Alternative methods for dispensing the etch barrier could include wetting the template. The template could be spin-coated with etch barrier and then pressed onto the wafer. Alternatively, a thin later of etch barrier could be painted onto the template before it is mated to a silicon wafer. Creative thinking in this area may sidestep some critical technical issues that could delay SFIL development

6.2.2 Scientific Investigation

The problem of minimizing excess etch barrier material leads one to consider a number of fundamental questions about the interface between the template and the wafer. What mechanisms dominate the filling process as the liquid etch barrier wets the surfaces of the template and wafer? What is the most effective means of wetting these surfaces? What forces dominate the behavior of the etch barrier as the template and wafer are pressed together? At the macroscopic level, shear forces in the liquid will expel it to the edges of the template, but what happens as the thickness of the etch barrier film approaches zero? Answers to these questions and others will lead to greater understanding of the SFIL process.

6.2.3 Sensing

Sensing issues will play a key role in the investigation of the interface of the template and wafer. Currently, the SFIL project possesses no means of measuring the distance between the template and wafer as they approach one another. Answering many of the questions posed in the previous section will require a sensing system to clarify the mechanics of the template-wafer interface during various steps of the SFIL process.

Capacitive sensors have been considered for measuring this gap distance, but optical systems would be easier to implement. Broad band interference sensors such as those to measure film thicknesses (DRM type tools) are well understood, but these systems can only measure gaps down to a few hundred nanometers. A sensing scheme that produces an interferogram of the gap between the template and the wafer would give the user more information than a single point sensing system. An interferogram could indicate particle contamination or waviness in the silicon wafer, but such a system is more complex than a single

point system. Researchers on the SFIL project are currently investigating these systems.

Sensing systems are needed for two purposes: investigating the behavior of the template-wafer interface and characterizing alignment during the actual imprint process. One could construct a test bed solely for the purpose of investigating the template-wafer interface. Such a testbed would probably incorporate an interferogram type sensor or a point sensor mounted on a precision x-y table. This arrangement would allow one to investigate the gap thickness between two substrates that have been pressed together. Data from this testbed may indicate that a set of point sensors is sufficient for alignment during the printing process. Again, an understanding of the behavior of the template, wafer, and etch barrier will be key to future progress in the development of the SFIL process.

6.2.4 Active and Passive Stages

The issue of active versus passive stages will likely have to be addressed before a practical step and repeat tool can be completed. Passive stages are simpler than active stages and offer very high repeatability for lower cost and complexity. Their simplicity makes them an elegant solution to orientation and alignment needs of the SFIL process if they work. However, an active orientation stage may be required to fully implement SFIL. If one wants to control the spacing of the template and wafer without making contact, an active stage is required. Furthermore, overlay will be difficult at best if an SFIL machine does not incorporate an active stage. It may be possible to predict the behavior of a passive stage, but one cannot alter the behavior of an passive stage during the imprint process, in other words, a passive stage cannot incorporate error correction and feedback into an operating scheme.

6.2.5 Overlay

To eventually see integrated circuits manufactured with SFIL, overlay must at least be considered during the development process. The decision to avoid high forces and high temperatures during the SFIL process implicitly acknowledges the importance of this subject. To construct a multi-layer semiconductor device, successive circuit layers have to be aligned or overlaid.

The SFIL project need not develop an overlay scheme to align numerous images, but it should consider the needs of an overlay scheme. For example, one may have to incorporate an active stage in an eventual SFIL stepper to achieve the desired overlay accuracy. To make the greatest possible contribution to SFIL development, mechanical stage design work should consider the needs of potential overlay systems.

6.2.6 Template Loading and Deformation

The method of holding the template during the imprint process may require further investigation. Simply clamping the template in a few places may significantly deform the template and distort and image written on the template. By avoiding high temperatures, SFIL avoids thermal expansion and contraction of the template. Deformation due to fixturing forces also merits consideration. This deformation may be enough to disrupt the operation of a circuit manufactured with SFIL. Overlay could also be affected by these distortions.

Appendix A

MATLAB Code to Compute Compliance Kinematic Model

The following file computes the compliance matrix, eigenvalues, and eigenscrews for the ideal kinematic model.

```
clear all
% threeD.m
% this routine finds the compliance matrix for a three legged parallel
linkage
% it then computes the eigenvalues and eigenvectors of the compliance
matrix

% Eigenscrew analysis of 3 DOF kinematic model of orientation stage
l = 1; % length of side of stage triangle

% Define spring compliances
d = zeros(6,6);
d(1,1) = 0; % denotes reciprocal wrench
d(2,2) = 0; % denotes reciprocal wrench
d(3,3) = 0; % denotes reciprocal wrench
d(4,4) = 1; % compliance of spring 1
d(5,5) = 1; % compliance of spring 2
d(6,6) = 1; % compliance of spring 3

% Define p and w vectors for each screw

p1 = [1/2;-sqrt(3)/6;0]*1;
p1r = p1;
p2 = [0;1/sqrt(3);0]*1;
p2r = p2;
p3 = [-1/2;-sqrt(3)/6;0]*1;
p3r = p3;
w1 = [1/2;sqrt(3)/2;0];
w2 = [-1;0;0];
w3 = [1/2;-sqrt(3)/2;0];
w1r = [0;0;1];
w2r = w1r;
w3r = w1r;

% Construct screws from p's and w's

pw1 = cross(p1,w1);
pw2 = cross(p2,w2);
pw3 = cross(p3,w3);
pw1r = cross(p1r,w1r);
pw2r = cross(p2r,w2r);
pw3r = cross(p3r,w3r);
```

```

s1 = cat(1,w1,pw1);
s2 = cat(1,w2,pw2);
s3 = cat(1,w3,pw3);
slr = cat(1,wlr,pwlr);
s2r = cat(1,w2r,pw2r);
s3r = cat(1,w3r,pw3r);

J = cat(2,s1,s2,s3,slr,s2r,s3r)

% Compute compliance matrix
C = ((inv(J')))*d*inv(J);
piop = [zeros(3),eye(3);eye(3),zeros(3)];
pC = piop*C;
[V,D] = eig(C);
[pV,pD] = eig(pC);

format short
C
disp('Pi times C:');
pC
disp('Eigenvalues of Pi times C:');
pD
disp('Eigenvectors of Pi times C:');
pV

```

Appendix B

MATLAB Code to Compute Compliance Matrix of Distributed Flexure Stage

This code computes a compliance matrix describing the displacement of the distributed orientation stage for a given applied wrench. Proc.m reads data node displacement data generated from an IDEAS finite element model. The data is formatted and passed to twist.m. Twist.m calculates a twist vector given two sets of points as input. The output from twist.m is then used to compute a compliance matrix.

```
% proc.m
% this file reads node displacement data files and computes a
twist vector
%   for every displacement field

% clear all values from memory and set display format to long
clear all;
format long e;

% read initial node locations
nodeloc = dlmread('nodeloc.txt',' ');
x0 = nodeloc(:,2:4);

% read displaced node locations
data = dlmread('data.txt',' ');

% parse node locations into 6 separate matrices
x1 = data(1:22,2:4);
x2 = data(23:44,2:4);
x3 = data(45:66,2:4);
x4 = data(67:88,2:4);
x5 = data(89:110,2:4);
x6 = data(111:132,2:4);

% select three points in each displacement field
s0(1,:) = x0(1,:);
s0(2,:) = x0(5,:);
s0(3,:) = x0(13,:);
s0 = s0'-[0,0,0;30,30,30;0,0,0];

s1(1,:) = x1(1,:);
```

```

s1(2,:) = x1(5,:);
s1(3,:) = x1(13,:);
s1 = s1' + s0;

s2(1,:) = x2(1,:);
s2(2,:) = x2(5,:);
s2(3,:) = x2(13,:);
s2 = s2' + s0;

s3(1,:) = x3(1,:);
s3(2,:) = x3(5,:);
s3(3,:) = x3(13,:);
s3 = s3' + s0;

s4(1,:) = x4(1,:);
s4(2,:) = x4(5,:);
s4(3,:) = x4(13,:);
s4 = s4' + s0;

s5(1,:) = x5(1,:);
s5(2,:) = x5(5,:);
s5(3,:) = x5(13,:);
s5 = s5' + s0;

s6(1,:) = x6(1,:);
s6(2,:) = x6(5,:);
s6(3,:) = x6(13,:);
s6 = s6' + s0;

% Compute twist vectors for all six displacement fields
tw1 = twist(s0,s1);
tw2 = twist(s0,s2);
tw3 = twist(s0,s3);
tw4 = twist(s0,s4);
tw5 = twist(s0,s5);
tw6 = twist(s0,s6);

% assemble twist matrix
twt = zeros(6,6);
tw = zeros(6,6);

twt(:,1) = tw1;
twt(:,2) = tw2;
twt(:,3) = tw3;
twt(:,4) = tw4;
twt(:,5) = tw5;
twt(:,6) = tw6;

tw(:,1) = twt(:,1);

```

```

tw(:,2) = twt(:,2);
tw(:,3) = twt(:,3);

% Subtract first three twists from last three twists if flag = 1
flag = 0;

if flag == 0
    tw(:,4) = twt(:,4);
    tw(:,5) = twt(:,5);
    tw(:,6) = twt(:,6);
end

if flag == 1
    tw(:,4) = twt(:,4)-twt(:,1);
    tw(:,5) = twt(:,5)-twt(:,2);
    tw(:,6) = twt(:,6)-twt(:,2);
end

%tw(4:6,4:6) = 0

% filter twist matrix by zeroing any translation smaller than 10
microns
% and zeroing any rotation smaller than 0.1 milliradian

flag = 0;
if flag == 1
    for j = 1:6
        for i = 1:3
            if tw(i,j) <= 0.0001
                tw(i,j) = 0;
            end
        end
        for i = 4:6
            if tw(i,j) <= 0.001
                tw(i,j) = 0;
            end
        end
    end
end
end

% Read load node locations
loadread = dlmread('loadloc.txt',' ');
loadloc1 = loadread(1,2:4);
loadloc2 = loadread(1,2:4);
loadloc3 = loadread(1,2:4);
loadloc4 = loadread(2,2:4);
loadloc5 = loadread(3,2:4);

```

```

loadloc6 = loadread(4,2:4);

% compute rho vectors for wrenches
rho1 = (loadloc1-loadloc1)';
rho2 = (loadloc2-loadloc1)';
rho3 = (loadloc3-loadloc1)';
rho4 = (loadloc4-loadloc1)';
rho5 = (loadloc5-loadloc1)';
rho6 = (loadloc6-loadloc1)';

% compute w vectors for wrenches
magn = 15*4.44822; %newtons
w1 = [1;0;0];
w2 = [0;-1;0];
w3 = [0;0;1];
w4 = [1;0;0];
w5 = [0;-1;0];
w6 = [0;-1;0];

% compute wrenches
wr1 = zeros(6,1);
wr2 = zeros(6,1);
wr3 = zeros(6,1);
wr4 = zeros(6,1);
wr5 = zeros(6,1);
wr6 = zeros(6,1);

wr1(1:3) = w1*magn;
wr2(1:3) = w2*magn;
wr3(1:3) = w3*magn;
wr4(1:3) = w4*magn;
wr5(1:3) = w5*magn;
wr6(1:3) = w6*magn;

wr1(4:6) = cross(rho1,w1)*magn;
wr2(4:6) = cross(rho2,w2)*magn;
wr3(4:6) = cross(rho3,w3)*magn;
wr4(4:6) = cross(rho4,w4)*magn;
wr5(4:6) = cross(rho5,w5)*magn;
wr6(4:6) = cross(rho6,w6)*magn;

% Assemble wrench matrix
wr = zeros(6,6);
wrt = zeros(6,6);

wrt(:,1) = wr1;
wrt(:,2) = wr2;
wrt(:,3) = wr3;
wrt(:,4) = wr4;

```

```

wrt(:,5) = wr5;
wrt(:,6) = wr6;

wr(:,1) = wrt(:,1);
wr(:,2) = wrt(:,2);
wr(:,3) = wrt(:,3);

% Subtract first three wrenches from last three wrenches if flag
= 1
flag = 0;

if flag == 0
    wr(:,4) = wrt(:,4);
    wr(:,5) = wrt(:,5);
    wr(:,6) = wrt(:,6);
end

if flag ==1
    wr(:,4) = wrt(:,4)-wrt(:,1);
    wr(:,5) = wrt(:,5)-wrt(:,2);
    wr(:,6) = wrt(:,6)-wrt(:,2);
end

% Compute pi operator matrix
p = [zeros(3),eye(3);eye(3),zeros(3)];

% Compute C
pC_num = tw*inv(wr);
C_num = p*pC_num;

% scale values of translations and rotations and compute C_num
again
flag = 1;
if flag ==1
    testCforce = [C_num(1,1),C_num(2,2),C_num(3,3)];
    testCmoment = [C_num(4,4),C_num(5,5),C_num(6,6)];
    a = max(testCforce)
    b = max(testCmoment)
    s = a/b

    twscaled = tw
    twscaled(1:3,:) = twscaled(1:3,)*s;
    twscaled

    pC_num = twscaled*inv(wr);
    C_num = p*pC_num;
end

% Make C symmetric if flag = 1

```

```

flag = 1;

if flag ==1
    C = 0.5*(C_num + C_num');
    C_noise = 0.5*(C_num - C_num');
else
    C = C_num
end

pC = p*C;

% Compute eigenvalues of C and pi*C
[V,D] = eig(C);
[pV,pD] = eig(pC);

% normalize eigenvectors if flag = 1;
flag = 1;
if flag ==1
    pV(1:6,1) = pV(1:6,1)/norm(pV(1:3,1));
    pV(1:6,2) = pV(1:6,2)/norm(pV(1:3,2));
    pV(1:6,3) = pV(1:6,3)/norm(pV(1:3,3));
    pV(1:6,4) = pV(1:6,4)/norm(pV(1:3,4));
    pV(1:6,5) = pV(1:6,5)/norm(pV(1:3,5));
    pV(1:6,6) = pV(1:6,6)/norm(pV(1:3,6));
end

% normalize length components of eigenvectors
flag = 1;
if flag ==1
    temp = max(pV(4:6,:));
    temp = max(temp)
    pV(4:6,:) = pV(4:6,+)/temp;
end

format short
% Calculate work done my each wrench
e1 = wr(:,1)'*p*tw(:,1)
e2 = wr(:,2)'*p*tw(:,2)
e3 = wr(:,3)'*p*tw(:,3)
e4 = wr(:,4)'*p*tw(:,4)
e5 = wr(:,5)'*p*tw(:,5)
e6 = wr(:,6)'*p*tw(:,6)

% Display symmetric C and noise component of C
C
%C_noise

% Display twists and wrenches
tw

```

```

wr

% Display C and its eigenvalues and eigenscrews
C
D
V

% Display Pi*C and its eigenvalues and eigenscrews
pC
pD
pV

```

The following function, `twist.m`, computes the screw representation of the displacement of a rigid body. The function reads initial and final positions of three points on the rigid body and outputs a twist.

```

function [twistout] = twist(si,sf)

% given three initial points and three displaced points, this file
% computes a corresponding twist vector

pli = si(:,1);
p2i = si(:,2);
p3i = si(:,3);

plf = sf(:,1);
p2f = sf(:,2);
p3f = sf(:,3);

% Compute rotation matrices
pinit = zeros(3,3);
pfin = zeros(3,3);

pinit(:,1) = p2i-pli;
pinit(:,1) = pinit(:,1)/norm(pinit(:,1));

pinit(:,2) = cross(pinit(:,1),p3i-pli);
pinit(:,2) = pinit(:,2)/norm(pinit(:,2));

pinit(:,3) = cross(pinit(:,1),pinit(:,2));
pinit(:,3) = pinit(:,3)/norm(pinit(:,3));

pfin(:,1) = p2f - p1f;
pfin(:,1) = pfin(:,1)/norm(pfin(:,1));

```

```

pfin(:,2) = cross(pfin(:,1),p3f - p1f);
pfin(:,2) = pfin(:,2)/norm(pfin(:,2));

pfin(:,3) = cross(pfin(:,1),pfin(:,2));
pfin(:,3) = pfin(:,3)/norm(pfin(:,3));

Qi = eye(3);
Qf = pinit*inv(pfin);

% Compute displacement vectors
qi = pli;
qf = plf;

% 1. compute g
g = qf - qi;

% 2. compute M and m
M = Qi*(Qf'); % <----- Remember this
m = qf-M*qi;

% 3. compute ctheta
ctheta = (M(1,1)+M(2,2)+M(3,3)-1)/2;
theta = acos(ctheta);

% 4. form l
l = zeros(3,1);
l(1) = M(3,2)-M(2,3);
l(2) = M(1,3)-M(3,1);
l(3) = M(2,1)-M(1,2);

% 5. compute ltm
ltm = l'*m;

% 6. determine sign(ctheta), compute sin(theta)
theta = theta*sign(ltm);
stheta = sin(theta);

% 7. form w
w = l/(2*stheta);

% 8. compute d
d = ltm/(2*stheta);

% 9. compute rho
I = eye(3);
rho = (I-M')*m/2/(1-ctheta);

% 10. compute h
h = d/theta;

```

```
% check to see if ctheta = 1 or ctheta = -1
%ctheta
%range = 0.05;
%if (1-range)<ctheta,(1+range);
%  disp('cos(theta) = 1 verify results');
%end
%if (-1-range)<ctheta,(-1+range);
%  disp('cos(theta) = -1 verify results');
%end

% assemble twist vector
twist = zeros(6,1);
twist(1:3) = w;
twist(4:6) = cross(rho,w) + w*h;
twistout = twist*theta;
```

References

- Badami, V. G., Smith, S. T., and Patterson, S.R., "A metrological three-axis translator and its application for constant force profilometry," *Proceedings of the Eleventh Annual Meeting of the American Society for Precision Engineering*, 1996, pp. 391-395.
- Choi, B. J., 1998, "Kinematic Design, Motion/Force Coordination, and Performance Analysis of Force Controlled Wheeled Vehicles", *Ph.D. Dissertation*, Mechanical Engineering, The University of Texas at Austin.
- Colburn, M., Johnson, S., Stewart, M., Damle, S., Choi, B.J., Bailey, T., Sreenivasan, S.V., Ekerdt, J., and Willson, C.G., "Step and Flash Imprint Lithography: An alternative approach to high resolution patterning." SPIE's 24th Intl. Symp. Microlithography: Emerging Lithographic Technologies III. March 14-19, 1999 Santa Clara, CA.
- Gere, J. and Timoshenko, S., *Mechanics of Materials*, Third Edition, *PWS Publishing Company*, Boston, 1990.
- Haisma, J.; Verheijen, M.; van der Huevel, K.; van den Berg, J.; "Template-assisted nanolithography: A process for reliable pattern replication". *J. Vac. Sci. Technol. B* 14(6) (Nov/Dec 1996)
- Hunt, K. H., 1990, "Kinematic Geometry of Mechanisms", *Oxford: Clarendon Press*.
- P. Ruchhoeft, M. Colburn, H. Nounu, S. Damle, S. Johnson, M. Stewart, T. Bailey, B. Choi, S.V. Sreenivasan, J. Ekerdt, J. C. Wolfe and C. G. Willson, "Patterning Curved Surfaces: Template Generation by Ion Proximity Lithography and Relief Transfer by Step and Flash Imprint Lithography", *J. Vac. Sci. Technol.*, B, Oct/Nov, 1999.

- Patterson, T., and Lipkin, H., "Structure of Robot Compliance," *ASME Journal of Mechanical Design*, Vol. 115, 1993, pp.576-580.
- Smith, Stuart, and Chetwynd, D.G., "Foundations of Ultraprecision Mechanism Design," *Gordon and Breach Science Publishers*, Philadelphia, 1992.
- Strang, Gilbert. "Linear Algebra and Its Applications," Harcourt Brace Jovanovich, Publishers, San Diego, 1988.
- Thompson, Larry F., Willson, C. Grant, and Bowden, Murrae J., *Introduction to Microlithography*, 2nd ed., American Chemical Society, Washington, DC, 1994.
- Waldron, K. J., Course Notes for ME 851 Kinematic Geometry of Mechanisms, The Ohio State University, 1993.
- Waldron, K. J., Raghavan, M. and Roth, B., "Kinematics of a Hybrid Series-Parallel Manipulation System," *ASME Journal of Dynamic Systems, Measurement, and Control*, Vol. 111, 1989, pp. 211-221.

Vita

Stephen Christopher Johnson was born in Tulsa, Oklahoma on December 8, 1974, the son of Carolyn Ann Johnson and James Massey Johnson. After completing his work at James E. Taylor High School in Katy, Texas, in 1993, he entered The University of Texas at Austin in Austin, Texas. He received the degree of Bachelor of Science from The University of Texas at Austin in August, 1997. In September, 1997, he entered The Graduate School at The University of Texas at Austin.

Permanent Address: 910 Kentbury Ct.
Katy, Texas 77450

This thesis was typed by the author.